NUMERICAL MODELING OF BLOOD FLOW IN HUMAN LEFT CORONARY ARTERY AND *IN VITRO* STUDY OF ENDOTHELIAL CELL ACTIVTION BY SHEAR STRESS

By

SARAVAN KUMAR SHANMUGAVELAYUDAM

Bachelor of Engineering in Mechanical Engineering

Anna University

Chennai, India

2007

Submitted to the Faculty of the
Graduate College of the
Oklahoma State University
in partial fulfillment of
the requirements for
the Degree of
MASTER OF SCIENCE
May, 2009

NUMERICAL MODELING OF BLOOD FLOW

IN HUMAN LEFT CORONARY ARTERY AND

IN VITRO STUDY OF ENDOTHELIAL CELL

ACTIVTION BY SHEAR STRESS

Thesis Approved:

Dr. Wei Yin

Thesis Adviser

Dr. David A. Rubenstein

Dr. David G. Lilley

Dr. A. Gordon Emslie

Dean of the Graduate College

To the greatest pioneers of science

ACKNOWLEDGMENTS

I would first like to acknowledge my advisor Dr. Wei Yin for her guidance, support, and patience. Her availability and willingness to assist with my research work helped me to complete this thesis. I specially want to thank her for the time she spent correcting my abstract, manuscript and thesis report.

I would like to thank Dr. David Rubenstein for his support and advice. I also want to thank Dr. David G. Lilley for serving on my thesis committee.

My parents Saradha and Shanmugavelayudam and my brother Karthik Kumar are my constant source of inspiration. None of this would have been possible without their unwavering support, love and faith.

I thank all my lab mates at BELOS, who made it a convivial place to work. I thank Mukund Subramaniam for being available to discuss my issues all the times. I extend my thanks to everyone who have helped and inspired me during my masters.

TABLE OF CONTENTS

LIST OF TABLES

Table Page

LIST OF FIGURES

Figure Page

CHAPTER I

INTRODUCTION

Coronary arteries are the blood vessels that supply blood to the heart muscles (myocardium). They are tethered to the surface of heart itself. The cardiac muscles need an uninterrupted supply of oxygen and nutrients. Any degenerative changes in coronary circulation will affect the cardiac blood supply and lead to reduced cardiac performance. Such chronic coronary condition is referred to as coronary heart disease (CHD). The reduced cardiac blood supply known as coronary ischemia usually results from the localization of atherosclerosis in coronary arteries. Atherosclerosis is a common vascular disease characterized by changes in the endothelial lining. The improper functioning of the endothelium leads to migration of lipids and leukocytes to the sub-endothelial layer. The continuous deposition of lipids and leukocytes at the sub-endothelial layer causes the plaque formation. The atherosclerotic plaque can induce the narrowing of blood vessel diameter and alters blood flow to the downstream region. The partial or complete blocking of coronary vessel leads to lack of oxygen supply to downstream region. The death of cardiac muscle in those regions due to insufficient oxygen refers to myocardial infarction (MI).

Atherosclerotic lesions are often localized to the left coronary arteries. The main branch of the left coronary artery (LCA) is the left main (LM) coronary artery.

LM bifurcates into the left anterior descending (LAD) artery and the left circumflex (LCX) artery. These arteries supply blood to both the left anterior region (LAD) and the left posterior region (LCX) of the myocardium (Figure 1.1), irrigating more than 50% of heart muscles (Kalbfleisch and Hort, 1977). CHD is the No.1 killer disease in the US (16.8 million deaths in 2006), accounting for more than 50% of cardiovascular disease (CVD) deaths (Figure 1.2, following page) (Lloyd-Jones et al., 2009).

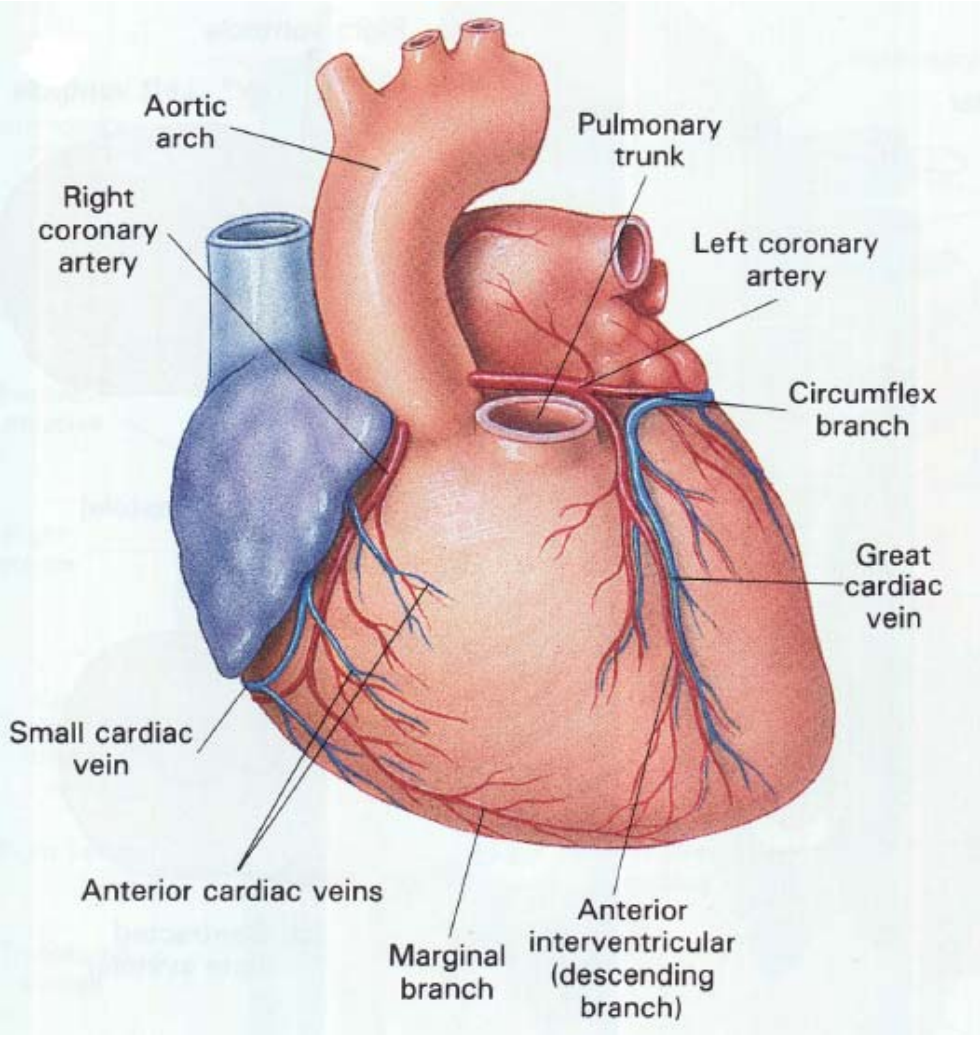

Figure 1.1 – A model of heart showing coronary circulation. The left anterior region is irrigated by the LAD and the posterior region is irrigated by circumflex branch (Martini, 1992).

The localization of atherosclerosis is generally governed by the action of hemodynamic forces on the endothelial cells. Hemodynamic shear stress (tangential force exerted by blood flow on vessel wall) and inflammation play very important roles in the initiation and propagation of atherosclerosis in coronary arteries. As the disease condition progresses, local shear stress conditions may change significantly, resulting in vascular wall endothelial cell damage (Fry, 1968), platelet activation and thromboembolism (Hellum, 1994). If a thrombus forms in coronary artery and blocks the blood supply to local cardiac muscles, the resultant ischemia (insufficient oxygen) can lead to MI (Willerson, 1995).

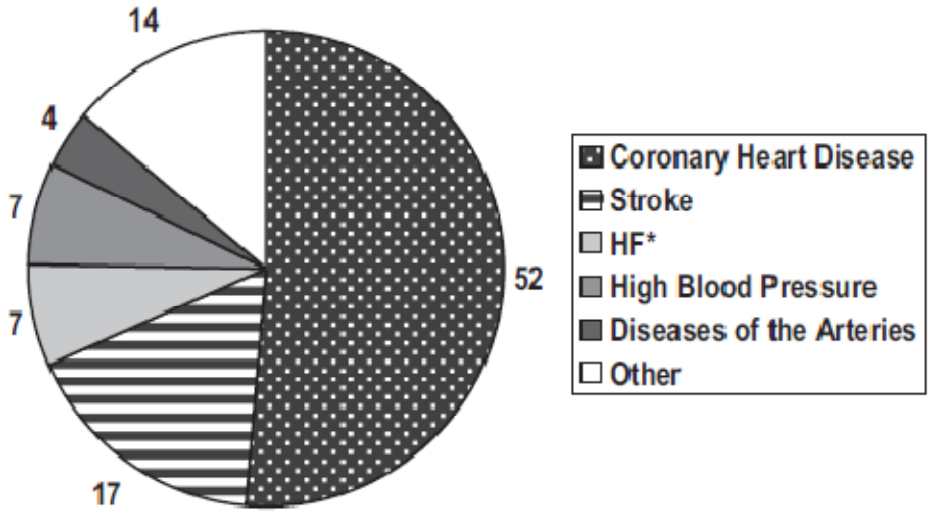

Figure 1.2 – Percentage breakdown of deaths due to CVD (United States, 2006) (Lloyd-Jones et al., 2009)

Endothelial cells (EC) form the innermost layer of blood vessels and are directly in contact with blood stream. Activation and dysfunction of EC may lead to many vascular diseases, which are closely related to hemodynamic shear stress induced by blood flow (Ridger et al., 2008). Therefore, it is essential to understand the response of EC to various shear stresses under physiological and pathological conditions.

It is well established that EC activation by shear stress and localization of atherosclerotic lesion are closely related. The lesions tend to localize to regions of disturbed blood flow with low and oscillating wall shear stress (WSS) patterns. These disturbed flow patterns are commonly found near an arterial bifurcation (Malek et al., 1999) and regions with complex vascular geometries such as those seen in coronary arteries.

This underlines the importance of studying the WSS magnitude and distribution in coronary arteries. A lot of numerical and *in vitro* models have been built to study the shear stress distribution in coronary arteries; however, most of them are limited by the use of simplistic geometrical models and flow assumptions, neglecting the realistic complexity in coronary arteries.

The aim of this study was to 1) develop a numerical model to estimate the shear stress distribution in the left coronary artery; 2) to apply estimated shear stress to EC to investigate their activities under physiological and pathological flow conditions. The results obtained from this study will improve our understanding of coronary blood flow and the activation and response of endothelial cells.

1.1 Objectives

The goal of this study was to present a clear picture of variation in shear stress distribution in the LAD close to the bifurcation. We also wanted to evaluate wall shear stress distribution in the left coronary artery and investigate its role on endothelial cell (EC) functions.

Global Hypothesis: Disturbed wall shear stress near the stenosis throat can activate endothelial cells and lead to inflammatory responses.

Specific Aim 1: To develop 2D and 3D models of the left coronary artery model with realistic geometries, under normal and stenosis conditions (30%, 60% and 80% severity). Flow field, velocity profiles and shear stress distribution will be computed using CFD.

Specific Aim 2: To apply the estimated wall shear stress to endothelial cells *in vitro* in a dynamic cone and plate shearing device to investigate the effect of altered WSS on EC activation and inflammatory responses.

This present project was a unique combination of computational and experimental work. The computational part of this work concentrated on developing coronary artery models (2D and 3D) with realistic geometries. The computational fluid dynamic analysis was carried out in these models with assumptions close to physiological conditions and the WSS distribution was compared between normal and disease conditions. Also, the results from CFD simulations were compared to establish the variation in WSS computed from 2D and 3D geometries. The shear stress history calculated from CFD was used in the cone and plate shearing device to mechanically stimulate EC. The goal of this study was to improve our present understanding of the role of shear stress in the pathogenesis

of atherosclerosis. The significance of this study would be to reveal the shear activation-response of EC, which may lead to better characterization of CHD and to improve clinical treatment.

CHAPTER II

BACKGROUND

2.1 Pathogenesis of atherosclerosis

The complex arterial geometries (curvatures and bifurcations) of the vascular system create regions of unique blood flow patterns. The pulsatile nature of the blood flow further adds to these complexities and produces regions of disturbed flow. Disturbed flow may promote reparative changes in the innermost layer of the artery wall – the intima. Endothelial cells (EC) present in this layer are sensitive to shear stresses induced by disturbed blood flow. Alternations in the wall shear stress (WSS) distribution may lead to endothelial activation and dysfunction. The low and oscillating flow affects the orientation of EC and leads to increased arterial wall permeability and modified surface protein expression (Sakamoto et al., 2006). Macromolecules, such as low density lipoprotein (LDL) can migrate through the endothelium and reach the sub-intimal space. The presence of LDL in the sub-endothelial layer can stimulate ECs to release increased amount of growth factors and adhesion molecules such as intercellular adhesion molecule - 1, vascular cell adhesion molecule - 1 and platelet endothelial cell adhesion molecule – 1 (Huo and Ley, 2001). This increased expression of adhesion molecules favors the adherence and migration of leukocytes (Springer, 1994). Thus, this localized sub-intimal accumulation promotes further recruitment of lipids and leukocytes at the same location and lead to the growth of atherosclerotic lesion.

2.1.1 Endothelial cells

Endothelial cells (EC) form the lining of the intimal layer. EC are sensate to shear stress variation. EC are found to be activated by certain disturbed WSS patterns and they respond through various biochemical pathways. One of the unique and earliest studies on EC behavior by shear stress revealed damage of EC when exposed to elevated shear for short period of time (Fry, 1968). The earliest response in the multistep process of atherosclerosis is the modulation in surface protein expression of EC (Davies et al., 1988). An injured endothelium amplifies the permeability to macromolecules compared to that of an intact layer (Huo and Ley, 2001; Penn et al., 1997).

Some *in vitro* studies have revealed the activation of EC at genetic levels. Investigations have shown either an increase or decrease in gene expression when EC are activated by varying shear stress (Ohura et al., 2003). This alters the normal cytokine release and protein expression on EC. Among all EC responses, increased surface adhesion molecule expression is of primary concern due to its role in leukocyte migration (Campbell et al., 1998).

An intact endothelium inhibits coagulation and thrombosis. On the other hand a damaged endothelium may actively promote coagulation and thrombosis due to the increased expression of tissue factor (TF) (Grabowski et al., 1993). An activated EC express both tissue factor (TF) and tissue factor pathway inhibitor (TFPI). EC under normal arterial levels of shear stress down regulate the surface TF expression (Grabowski et al., 2001). The major inflammatory response of EC to disturbed shear flow is an increase in TF expression (Lin et al., 1997). TF can initiate the coagulation cascade and lead to thrombus formation while TFPI inhibits coagulation. During the later stages of

atherosclerosis, TF expression governs the formation of clots. Certain *in vivo* studies have revealed an increased localization of TF in atherosclerotic plaque compared to that of normal vasculature (Wilcox et al., 1989). As the relationship between shear stress and atherosclerosis is well established, it is important to understand the surface expression of TF on EC under altered (disease) hemodynamic conditions.

2.1.2 Adhesion molecules

The important stage in the inflammatory response of EC is the leukocyte adhesion and infiltration mediated by adhesion molecules. These include selectins (P, E and L – Selectins) and immunoglobulins. Some of the important immunoglobulins include intercellular adhesion molecule 1 (ICAM-1), vascular cell adhesion molecule 1 (VCAM-1) and platelet endothelial cell adhesion molecule (PECAM-1). The selectins majorly assist in initial capture, roll and loose attachment of leukocytes to the EC layer at the disturbed flow regions (Huo and Ley, 2001). The firm adherence and trans-endothelial migration of leukocyte are facilitated by ICAM-1 and VCAM-1.

2.2 Intercellular adhesion molecule 1 (ICAM-1)

ICAM-1 is a transmembrane glycoprotein, present on the surface of EC. ICAM-1 is made up of (extracellular) immunoglobulin G (IgG) like domains (five) and a short cytoplasmic tail. Normal intact endothelium express low levels of ICAM-1 compared to that of injured endothelium (athero-prone sites) (Matthias et al., 1997). Examination of coronary arteries has revealed an increase in ICAM-1 expression near the lesions (Davies et al., 1993). In general, EC express higher levels of ICAM-1 when they are activated.

In the pathogenesis of atherosclerosis, ICAM-1 plays a major role in trans-endothelial migration of leukocytes (Yang et al., 2005). ICAM-1 on EC surface acts as a

ligand for leukocyte function associated antigen-1 (LFA-1) (commonly found in leukocytes) (Rothlein et al., 1986). Blocking experiments using monoclonal antibodies for both ICAM-1 and LFA-1 have revealed a significant variation in leukocyte adhesion. Also, activated EC with increased ICAM-1 expression revealed an increase in leukocyte migration compared to resting cells (Dustin and Springer, 1988; Roos and Roossien, 1987). Leukocyte adhesion to EC is one of the earliest cellular responses in atherosclerosis.

The two major factors that affect ICAM-1 expression are activation of EC by cytokines and shear stress. Some of these cytokines are released by macrophages that infiltrate the endothelium. In general, the plasma level of cytokines is significantly higher in patients with coronary artery disease (Tentolouris et al., 2004). When treated with cytokines including Tumor Necrosis Factor –α (TNF-α), Interferon-γ (IFN-γ) and Interleukin-1 (IL-1), EC become activated (Pober et al., 1986). These activated EC have shown a time dependent upregulation of ICAM-1 (Bevilacqua et al., 1994).

Apart from cytokine stimulation, mechanical shear stress is also found to induce ICAM-1 expression. The study conducted by Nagel et al., shows an upregulation of ICAM-1 surface expression when EC are exposed to a constant shear of 1Pa for 48hrs (Nagel et al., 1994). Similar patterns of ICAM-1 distribution was found when the cells are exposed to low constant shear of 0.3Pa and a varying shear pattern between 0.25 and 4.5Pa over a period of 24hrs (Nagel et al., 1994). Frattini et al., reported that both laminar (0.4 or 1.1Pa) and turbulent flows (orbital shaker, 210 rpm; center, 0.4Pa; periphery, 1.1Pa) induced similar amount of ICAM-1 on the EC surface (Frattini et al., 2004). This suggests that the EC activates similarly to various shear stress levels or that different

activation pathways converge down to similar responses. The study conducted by Sucosky et al., revealed an upregulation of ICAM-1 when aortic EC were exposed to unidirectional pulsatile flow (Sucosky et al., 2009). Chappel et al., treated EC with oscillatory shear stress (between +0.5 and -0.5 Pa) for a period of 24 hrs. The oscillatory shear stress was found to have increased ICAM-1 expression (11 fold) (Chappell et al., 1998). In a study by Nagel et al., EC exposed to laminar shear stress (0.25 – 40.6Pa) for 48hrs, revealed a time dependent but force independent increase in surface ICAM-1 (Nagel et al., 1994). The study conducted by Morigi et al., revealed a significant time dependent increase in surface expression of ICAM-1 on human umbilical vein endothelial cells (HUVEC) when exposed to a laminar constant shear of 0.8Pa (for 6 hrs) (Morigi et al., 1995). Meanwhile, the ICAM-1 expression remained unchanged when EC were exposed to a turbulent shear stress (average shear of 0.86Pa). Furthermore, the study by Tsuboi et al. indicated that when HUVEC were exposed to a constant shear of 1.5Pa (4 hrs), surface ICAM-1 expression increased to 1.27 times that of control (no shear) (Tsuboi et al., 1995). The mRNA quantification through PCR analysis showed a similar upregulation with parallel time course to that of surface expression.

In terms of shear stress activation, most of the *in vitro* studies have shown an upregulation of ICAM-1 when EC are exposed to constant laminar shear stress (mostly between 1-2Pa). However, this ICAM-1 observation contradicts the result from *in vivo* studies on ApoE-deficient mouse conducted by Nakashima et al. In their study, ICAM-1 was upregulated on EC surface at lesion prone sites bearing disturbed flow (Nakashima et al., 1998).

Besides these variations between *in vitro* and *in vivo* observations, most of *in vitro* studies used constant shear stresses which were not physiological. In vitro studies with more realistic physiological shear stress waveforms are urgently needed to investigate the effect of shear stress on ICAM-1 expression.

2.3 Tissue Factor

Tissue factor (TF) is a membrane bound glycoprotein synthesized by EC and leukocytes. TF serves as a cofactor for Factor VII/VIIa in initiation of coagulation cascade. The major function of TF is to maintain the blood hemostasis during vessel injury. EC releases soluble TF and expresses surface TF when activated or injured. During inflammation (atherosclerosis) there has been an over production of TF near regions of plaque, which plays a significant role in thrombosis associated plaque rupture (Wilcox et al., 1989). The TF expression is generally measured by the production of factor Xa.

The EC exposed to a constant laminar shear stress of 1.5Pa showed a time dependent increase in TF gene expression (5 fold increase) (Houston et al., 1999). In the study conducted by Grabowski et al., EC expressed a down regulation of TF at the mRNA level when the cells are sheared at 0.068 or 1.32Pa compared to cells that are not sheared (Grabowski et al., 2001). The common underlying reason behind the modulation in TF expression was found to be the amount of TFPI released by EC which is also governed by hemodynamic shear stress. This was confirmed in a study by Grabowski et al., EC expressed an increased amount of TF expression in the presence of an inhibitor of TFPI (Grabowski et al., 1993). The study by M C Lin et al., reported a transient increase in TF procoagulant activity in HUVEC exposed to constant shear of 1.2Pa. There was an

increase in both factor Xa formation and also mRNA levels of TF. The TF expression was very high after 6 hrs of shearing and went back to basal levels after 12 hrs of shearing (Lin et al., 1997).

Together, the expression of TF on activated endothelial cells is a sign of inflammation. The results from these studies indicate the dependence of TF expression on WSS. Again, most of these studies used a constant shear stress to activate EC. It is our interest to study EC surface TF expression when they are activated by physiologically relevant shear stresses.

2.4 *In vitro* activation of endothelial cells

A number of studies have been performed to characterize the functions of EC in normal and activated state. Some of them observed EC response when activated by mechanical stimulation (majorly shear stress) and chemical agonists (such as TNF-α, IFN-β, IFN-γ, etc). Endothelial surface ICAM-1, VCAM-1 and PECAM-1 expression are usually measured to determine EC activation level Soluble protein released from endothelial cells (like soluble tissue factor, soluble ICAM-1) and selectins (P-selectin, E-selectin) can also be used as a measure of endothelial activation. Immunofluorescence microscopy, western blotting and ELISA are common techniques that are used for endothelial activation measurement.

A cone and plate viscometer can be used to apply precisely controlled shear stress to endothelial cells. In the present study, we used a cone and plate shearing device to generate physiologically relevant shear stress to mimic *in vivo* shear loading conditions for EC (based on Brett Blackman's original design (Blackman et al., 2000)). The cone and plate hemodynamic cell shearing device is comprised of a cone which rotates over a

stationary base plate (holds the cultured monolayer of cells). This device helps in replicating an accurate arterial shear stress pattern based on the input parameters (Buschmann et al., 2005). By adjusting the cone angle and the rotating speed of cone, a variety of range of shear stress can be generated (Bussolari et al., 1982). This device was used in previous studies to produce a physiological laminar shear stress pattern found in arteries under normal conditions (Bussolari et al., 1982; Dewey, Jr. et al., 1981).

Initial *in vitro* experiments conducted with cone and plate devices confirmed the shear stress associated morphological changes in EC, changes in cell stiffness, proliferation and migration. In 1985 Frangos et al. found a two fold increase in prostacyclin released by EC exposed to pulsatile shear stress compared to that of EC activated by normal steady shear stress (Frangos et al., 1985). Subsequent analysis by many researchers revealed regulation of several effector molecules, coagulation factors, cytokines, and vasoactive substances released by EC governed by the activation of shear stress. The endothelial cells were later found to increase the release of transcription factors like nuclear factor (NF-κB), early growth response-1 (Egr1) and activator protein-1 (Ap-1) when exposed to disturbed shear stress than the normal shear stress (Nagel et al., 1999). These results satisfactorily reproduce the *in vivo* inflammatory response of EC to shear stress. This substantiates the use of cone and plate devices to study the shear stress activation-response of EC, which was investigated in this study. The surface protein expression (ICAM-1) was quantified based on an immunofluorescence technique and was used as a measure of EC activation. Using a similar technique, the inflammatory response of EC was measured based on the amount of surface TF expression when exposed to physiologically relevant shear levels.

2.5 Hemodynamics of atherosclerosis

Mechanical stresses can alter the internal cell signaling in EC and lead to their activation. The responses include chemokines and protein release leading to lipid and leukocyte accumulation and formation of lesion. These lesions anchor to regions which share a particular hemodynamic similarity. Based on these similarities, certain regions in vasculature were defined as athero-prone regions. These include the coronary artery, carotid artery, terminal abdominal aorta and their major branches. The lesions tend to form near the entrance of branch or the bifurcation of a parent vessel into daughter vessels. These regions of vasculature share a complex disturbed blood flow behavior.

Some of the important fluid dynamic characteristics that have been suggested to play a role in atherogenesis include flow separation, formation of recirculation zone, vortex formation and separation, spatial and temporal gradients of shear stress (Asakura and Karino, 1990). Most of these factors are commonly found near the bifurcation and downstream the stenosis throat region. The flow separation near the bifurcation creates region of disturbed flow downstream the bifurcation with high velocity gradient. Downstream of the stenosis throat the flow separates and forms recirculation zones. Platelets in the blood stream that get trapped within this zone are expected to be in contact with the endothelium for longer than normal durations. These cells when exposed to the disturbed hemodynamic region may get activated and cause further complications. The fluid dynamics of coronary artery has received much attention because of the disturbed coronary flow patterns and the flow induced inflammatory response in endothelial cells. The major hemodynamic property that has been extensively studied is

the wall shear stress (WSS). The variation in WSS has a direct impact on the activation and the response of endothelial cells and plays a key role in the localization of lesions.

In the case of Newtonian fluids, the shear stress is proportional to strain rate with viscosity being the constant of proportionality.

$$\tau \propto \frac{du}{dy}$$

Where τ is the shear stress and $\frac{du}{dy}$ is the strain rate (2D).

Similarly, in the case of Newtonian fluids, the wall shear stress is the product of viscosity times the velocity gradient at the artery wall.

$$\tau_w = \mu_{eff} \frac{du}{dy}$$

Where τ_w is wall shear stress, μ_{eff} is the effective viscosity (in case of laminar flow it is the molecular viscosity and in case of turbulent flow it is the sum of turbulent and laminar viscosity) and $\frac{du}{dy}$ is the velocity gradient at y = R (R is the radius of the blood vessel) in a direction tangential to the direction of blood flow.

Blood behaves as a continuous fluid medium, despite its formulation of blood cells and proteins, in large arteries. Hence it is valid to assume blood as a continuous fluid (single phase) when the arteries under consideration are large (around 4mm or more in diameter).

There are two very contradicting hypotheses relating shear stress to the localization of atherosclerotic lesions. The first implicated that high shear stress caused endothelial damage/erosion which eventually leads to the exposure of sub-endothelial layer to the blood stream (Fry, 1969). The sub-endothelial layer is sticky and blood components like leukocytes and platelets directly stick to this layer. The other hypothesis

indicated that the activation of EC occurs at low shear stress and that leads to the lesion growth (Caro et al., 1971). Several studies that have been conducted in the past 3 decades have confirmed the low shear hypothesis. The WSS in the predisposed places of atherosclerotic importance is significantly lower in magnitude and exhibit directional changes (Asakura and Karino, 1990; He and Ku, 1996; Jeremias et al., 2000).

WSS is a vector which acts in a direction parallel to the local velocity vector near the wall. The levels of vascular WSS are normally in the range between 0.5 and 2Pa and can instantaneously rise to 4Pa during increased cardiac output in large arteries (such as coronary artery, carotid artery, and iliac artery) near the bifurcations. In the locations of unique geometrical features including the bifurcation, curvature and branches the flow separates from the wall, creating a highly disturbed flow pattern with formation of eddies and vortices. Some of the *in vitro* studies have revealed that the shear stress instantaneously changes direction (opposite to the direction of flow). The magnitude can vary largely in areas of flow separation, reaching a peak value of 4Pa near the point of separation and just after the flow reattachment. This trend has been observed in carotid artery bifurcation (Motomiya and Karino, 1984; Zarins et al., 1983), coronary artery bifurcation (Asakura and Karino, 1990), infrarenal and femoral artery vasculatures (Pedersen et al., 1997).

2.6 Coronary artery

Tethered to the surface of heart the coronary arteries undergo the same movement of the heart and perform the major function of supplying oxygen to the cardiac muscles. These arteries originate from the base of aorta and the principle branches are the left (LCA) and the right coronary artery (RCA). The LCA originates from the left aortic sinus

and it irrigates nearly 68.8% of cardiac muscle mass and 79% of left ventricle muscle mass (Kalbfleisch and Hort, 1977). The primary constituents of LCA are left main (LM) artery which bifurcates into left anterior descending (LAD) and left circumflex (LCX) coronary arteries. The average diameter of LCA is around 4mm (Figure 2.1, Following page).

The rate of blood flow inside coronary arteries is highly variable and it depends on the oxygen requirement of the myocardium. The cardiac pulsatile flow inside the coronary artery is exactly opposite to the rest of the circulatory system. During systole, when the heart muscles contract and pump blood through the aorta, the flow reverses in the coronary artery (due to the high pressure gradient near the base of aorta). During diastole, the heart muscles are relaxed and the majority of coronary flow occurs with the peak average inlet velocity of about 15cm/sec (Chandran et al., 2007a).

The coronary artery shares one of the most complex vasculature involving twists, bends, taper and bifurcation. These geometrical factors are known to produce disturbance in flow and can affect the shear stress distribution, thereby governing the localization of lesions (Iwami et al., 1998). The study conducted by Asakura et.al., using flow visualization and high speed cinemicrographic techniques, revealed the complex flow patterns in the left and right coronary arteries with distinct regions of disturbed flow (Asakura and Karino, 1990). Among all other branches of coronary artery, the left coronary artery bifurcation is complicated by several important features (Bargeron et al., 1988). The length of LM artery is very small compared to that of other branches.

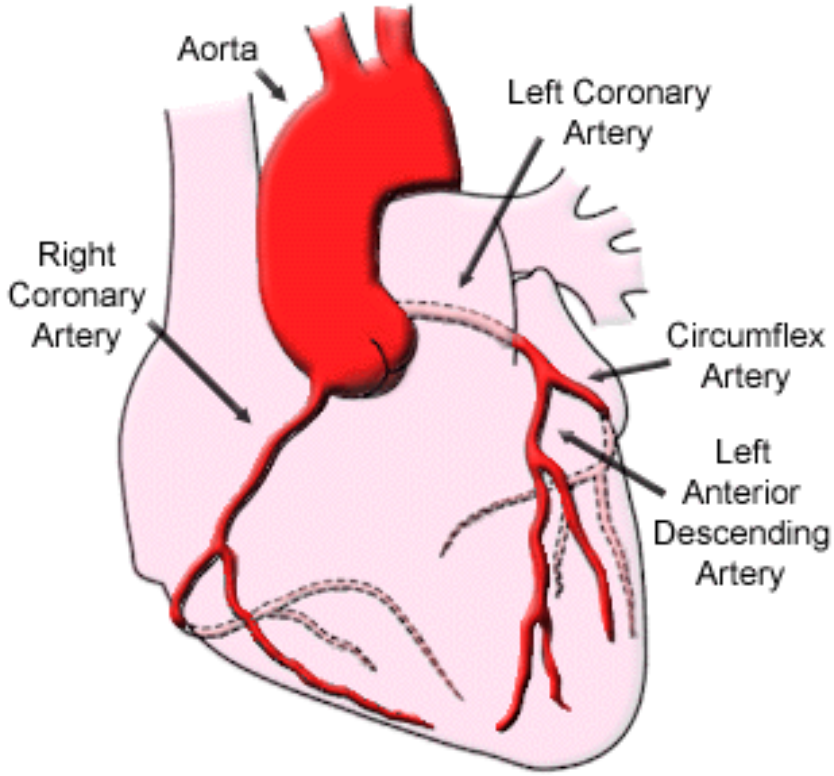

Figure 2.1 – The coronary artery on the myocardium with LM, LAD and LCX originating from the base of aorta.

The bifurcation in the left main artery does not lie in a single plane but replicates the curvature of the heart while branching. This might induce secondary flow formation during part of cardiac cycle. Moreover, the oscillation in shear stress in LCA has a strong correlation with the probability of plaque and focal location of atheroma (He and Ku, 1996).

Thus the composite environment of intricate geometry and flow behavior provides a combination of atherogenic and atheroprotective stimuli assisting the heterogeneous distribution of lesions independent of systemic risk factors. The analysis of hemodynamics in this set of arteries will provide a better understanding of fluid dynamics of blood under physiological and pathological conditions.

2.7 Computational Fluid Dynamics

The numerical analysis of blood flow is critical in understanding the role biomechanical stress plays in the pathophysiology of atherosclerosis. The notable variation in anatomy and very little information of the flow behavior in coronary arteries make hemodynamic studies on the coronary arteries challenging. The systems like Laser Doppler Anemometer (LDA), pulsed Doppler ultrasound and hot film anemometer have been used before to study the velocity distribution *in vivo*. These instruments can predict important flow characteristics but cannot directly measure the shear stress distribution. Despite their direct measurements, these are performed only at limited sites and the shear rates are difficult to estimate from near wall velocity measurements. Also, these techniques are very time consuming, which limits the ability to explore effects of variation in anatomy and flow waveform.

Computational Fluid Dynamics (CFD) is a unique and effective tool to model and predict blood flow conditions inside coronary arteries. CFD has the flexibility of accommodating changes in arterial geometry and pulsatile flow conditions. It can provide accurate results with very high spatial and temporal resolutions. The velocity of all the fluid cell elements within the artery can be calculated. A highly accurate shear rates both in magnitude and distribution at all surfaces can also be calculated. CFD provides a reliable platform for a time varying 3D flow patterns in a complex geometrical model, which can help to provide important information in investigating the effects of mechanical stress on coronary heart diseases.

2.8 CFD of coronary flow

A number of studies have been conducted to investigate blood flow in coronary arteries. The major hemodynamic properties that have been under consideration are velocity profile, pressure gradient and shear stress magnitude and distribution. Some of the common fluid dynamic similarities found in most of these studies are listed below.

The velocity profile near the bifurcation is skewed towards the flow divider (inner) wall. This created regions of high wall shear stress at these sites compared to surrounding locations. Also, the intensity of skewness varies during one cardiac cycle. During the deceleration phase, the flow separates with low retrograde velocities formed at the outer walls of branching region. This creates a complex shear stress distribution in both branches. The flow inside the branches after several diameters downstream relaminarizes and attains a fully developed flow.

Most of the CFD analysis of coronary flow use simple geometries. These geometries generally neglect the taper of arteries, the complex bends and the myocardial curvature of LCA. The result from the study conducted by He et al., revealed a time averaged WSS variation from about 0.3 to 9.8Pa inside the LCA(He and Ku, 1996). The model used in this study was a simplified 3D LCA with a monoplane bifurcation in physiological dimensions; also the LAD and LCX were of constant diameter and exactly perpendicular to the plane of bifurcation. The spatially averaged shear stress near the inlet of LCA was computed to be around 3.5Pa and dropped to 2Pa before the flow reached the bifurcation. Downstream the bifurcation the flow in LAD reached the value around 2.3Pa and in LCX 1.73Pa. The distribution of WSS on both the inner and outer wall was similar to that of other studies.

A similar study conducted by Perktold et al., used a more realistic coronary artery model rebuilt based on dimensions of an artery acquired from autopsies (Perktold et al., 1998). This model replicated the LAD only to the first diagonal branch and not the entire artery. A pulsatile inlet waveform obtained from Laser Doppler was used. They showed that the average shear stress before the bifurcation was around 0.42Pa and as the flow developed downstream the average WSS on LAD was 1.14Pa and that in the LCX was 1.12Pa. Besides these studies that have calculated the shear stress under normal conditions, there are considerable amount of work into hemodynamics under disease conditions. These studies aim at characterizing the flow and shear stress distribution around the stenosis throat region. The most famous model of stenosis geometry was that of Giddens et al. (Ahmed and Giddens, 1984). Varghese et al. used this stenosis geometry to study the pulsatile turbulent flow across the throat region (Varghese and Frankel, 2003). The maximum WSS just before the throat region went as high as 120Pa and dropped immediately to normal levels of around 2Pa just downstream the throat.

The CFD analysis from simple curved stenosis geometry showed a similar skewing of velocity towards the outer wall of curvature (Yao et al., 2000a). This study by Yao et al., compared the variation in peak shear stress calculated from coronary artery models with varying bend and stenosis severity (throat center at the center point of bend). The results showed that the WSS value was more dependent on the stenosis severity than the variation in bend angle. The peak WSS at the stenosis throat reached 300Pa in models with 60˚ and 120˚ bend.

The study conducted by Nosovitsky et al. compared the shear stress distribution in a simplified curved coronary artery model with and without stenosis (Nosovitsky et al.,

1997a). Under steady conditions, the maximum WSS peaked at 70Pa, whereas in unsteady simulations the maximum WSS varied between low (opposite direction) and 125Pa within a cardiac cycle at the stenosis throat. The disturbed WSS distribution was similar in all stenosis conditions, except that the magnitude increased with increasing stenosis severity.

Giannoglou et al. used a more realistic model based on the intrathoracic spatial measurement of coronary artery of a normal heart (Giannoglou et al., 2005). Locally low wall pressure and shear stress gradient was computed at the anatomic sites close to the bifurcation downstream in the LAD. This study revealed higher shear stress gradient at bifurcation and branching locations with the formation of vortices and secondary flow.

The study conducted by Farmakis et al. used the same model from Giannoglou et al. (Farmakis et al., 2004). The contours of WSS gradient showed regions of high and low shear occurring in a short axial distance near the wall of bifurcation and branching, creating a region of highly dynamic shear stress variation. These two studies were based on steady flow assumption which neglected the prediction of time dependent variation in shear stress distribution.

The results from all the above mentioned studies indicated a large variation in the shear stress estimation using CFD. These differences arise due to the various geometries used in these studies. Despite the resemblance in the distribution of WSS predicted by all these studies, they vary significantly in magnitude. Also, most of these studies assumed a steady flow condition despite the fact that the actual blood flow is pulsatile. This steady flow assumption rules out the possibility of estimating the shear stress history within one cardiac cycle that a particular region of endothelium is exposed to. The shear stress

history is one of the key parameters for *in vitro* studies to understand the mechanical force activation of EC. In this study we used both a simple 2D model and a complex realistic 3D model to compute the shear stress history based on physiological assumptions.

CHAPTER III

MATERIALS & METHODS

3.1 Numerical Simulation

3.1.1 Modeling of Coronary artery

The model of the left coronary artery (LCA) was developed using the computer aided designing (CAD) software Pro-E Wildfire 3.0 (PTC). In this study we developed both 2D and 3D models of LCA to study blood flow dynamics under normal and disease conditions (stenosis). For stenosis models, we induced a 30%, 60% and 80% reduction in vessel diameter.

The dimensions and the geometrical information of the arteries used in our models were obtained from Dodge's report (Dodge, Jr. et al., 1988a; Dodge, Jr. et al., 1992a). In their study, the intrathoracic spatial location of specific coronary artery segments was measured on a normal human heart based on angiographic imaging. Dodge et al., presented an accurate measurement of the centerline trajectory of LM, LAD, LCX and their branches using spherical coordinates and the diameters of each vessel at different cross sections along the trajectory. This provided a way to replicate the myocardial curvature of the coronary artery in a realistic manner, which accounts for bifurcation, curves and taper.

These spherical coordinates (Appendix A) were used to model the centerline trajectory of the LCA. The various cross sectional diameters were then used to extrude the artery model in Pro-E. The LCA branches in the 2D and 3D model shared approximately similar length, bifurcation angle and degree of taper except for the complex curvature present in the 3D model. The geometrical details of both the 2D and 3D model are presented in Table 1. Figure 3.1 depicts both the 2D and 3D LCA model developed and used for the CFD analysis in this study.

The disease conditions were modeled in LAD by adding a stenosis throat in the flow domain. The lumen narrowing (center point of stenosis throat) occurred downstream of the bifurcation in the LAD branch, 8mm from the center point of bifurcation with the length of the throat varying between 4 to 9mm. The throat diameters and the geometrical locations of stenosis throat of all disease models were presented in Table 2.

Table 1 – Geometrical parameters of 2D and 3D LCA model used in this study

	Parameters	2D (mm)	3D (mm)
LM	Inlet Diameter	4.5	4.5
	Length	11	11
LAD	Inlet Diameter	3.8	3.8
	Length	120	118
	Outlet Diameter	1.9	1.9
LCX	Inlet Diameter	3.7	3.7
	Length	80	76.8
	Outlet Diameter	1.7	1.7
Bifurcation Angle		75˚	74.83˚

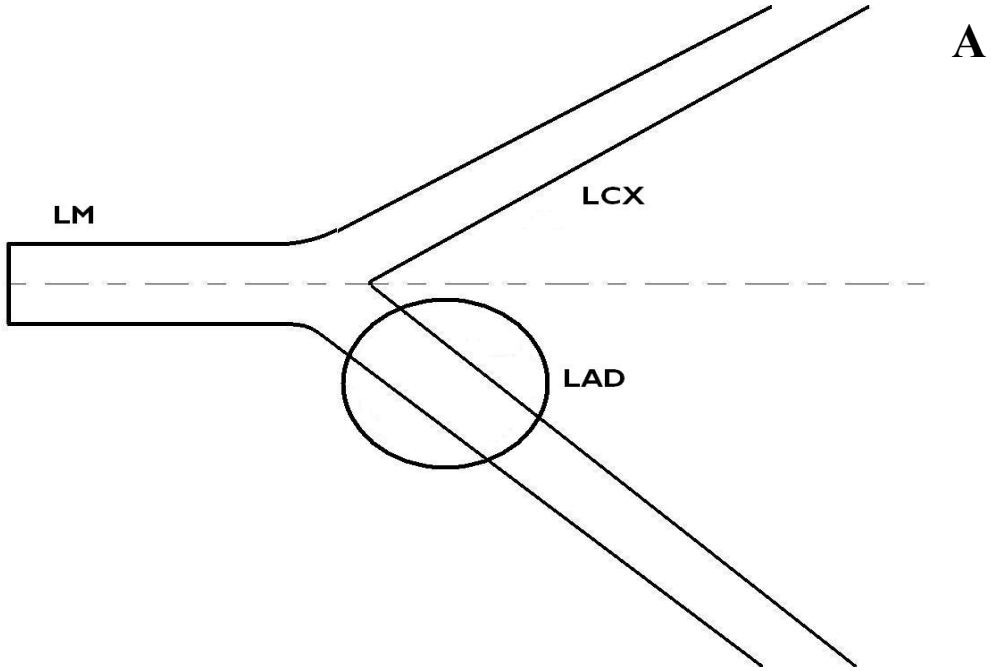

(A) – 2D model of LCA with three main branches similar to that of 3D model (circled portion – region of interest, location of stenosis)

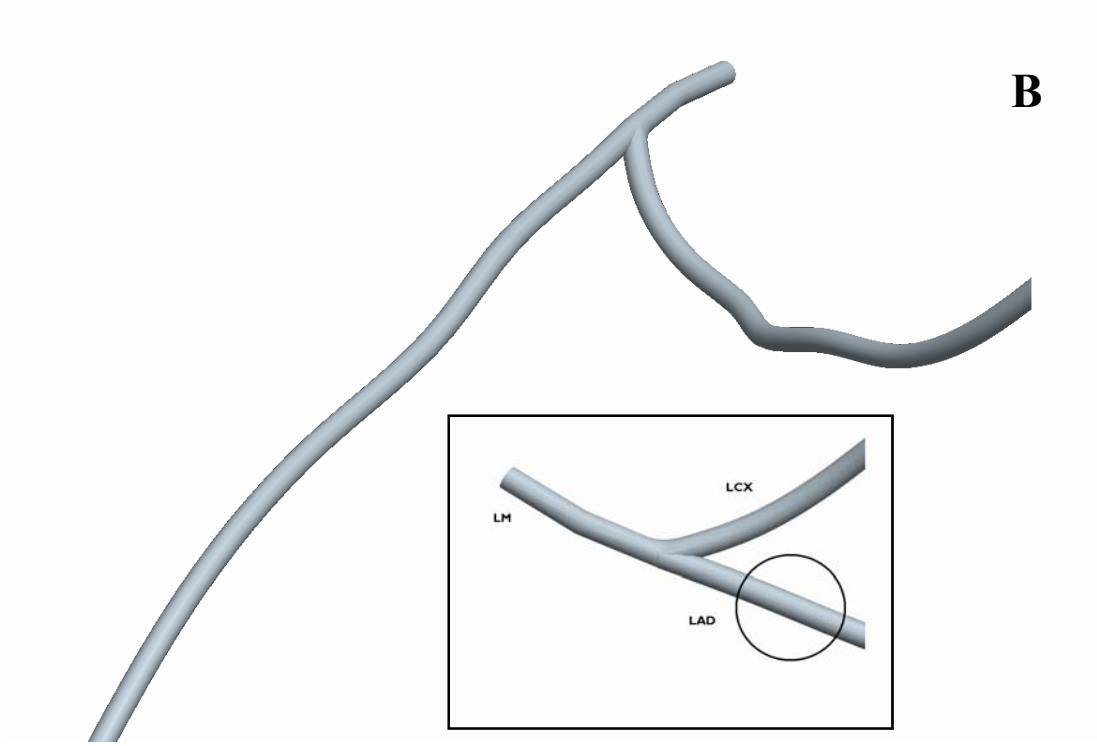

(B) –3D model of left coronary artery under normal condition. Inset picture shows the three main branches LM, LAD and LCX. The circled portion is the region of interest.

Figure 3.1 - 2D and 3D models of LCA (normal geometry) generated in Pro-E

Table 2 – Diameter of lumen at the center of stenosis throat at various disease conditions. Location information of stenosis throat (beginning, center and end point from the center point of bifurcation) in LAD under different stenosis severity conditions.

	Diameter (mm)	Throat location from bifurcation (mm)		
		beginning	center	end
30% Stenosis	2.59	6	8	10
60% Stenosis	1.492	5.5	8	10.7
80% Stenosis	0.74	3.5	8	12.8

3.1.2 Meshing

The models were discretized into small computational grids using Gambit v2.4.6 (ANSYS), the preprocessor program for CFD solvers. An unstructured mesh containing both quadrilateral and triangular elements was used in the 2D models. Since a quadrilateral mapping scheme would have resulted in a bad distorted mesh due to the presence of throat and bifurcation, the main region of interest (downstream the bifurcation in LAD branch near the stenosis region) was isolated from the rest of the model. An unstructured mesh with triangular elements (using pave scheme) was used to obtain a higher local resolution inside this region. The 2D models with mesh are shown in Figure 3.2.

Similarly the 3D models were meshed (Figure 3.3) with a hybrid mesh scheme using both hexahedral and tetrahedral elements. Regions of interest (bifurcation and stenosis throat region) were finely meshed with hexahedral or wedge elements using cooper volume mesh scheme. The numbers of elements used in all the models are listed in Table 3. For 3D models with 60% and 80% stenosis, fewer elements were used to compensate for the deficiency in computational memory, while using turbulent solvers. However, the cell density in the region of interest maintained the same. Boundary layers were attached to the wall in all models near the bifurcation region (region of interest where high velocity gradients develop) to provide more spatial and temporal resolution near the wall. All results from this study were checked and found to be independent of mesh density.

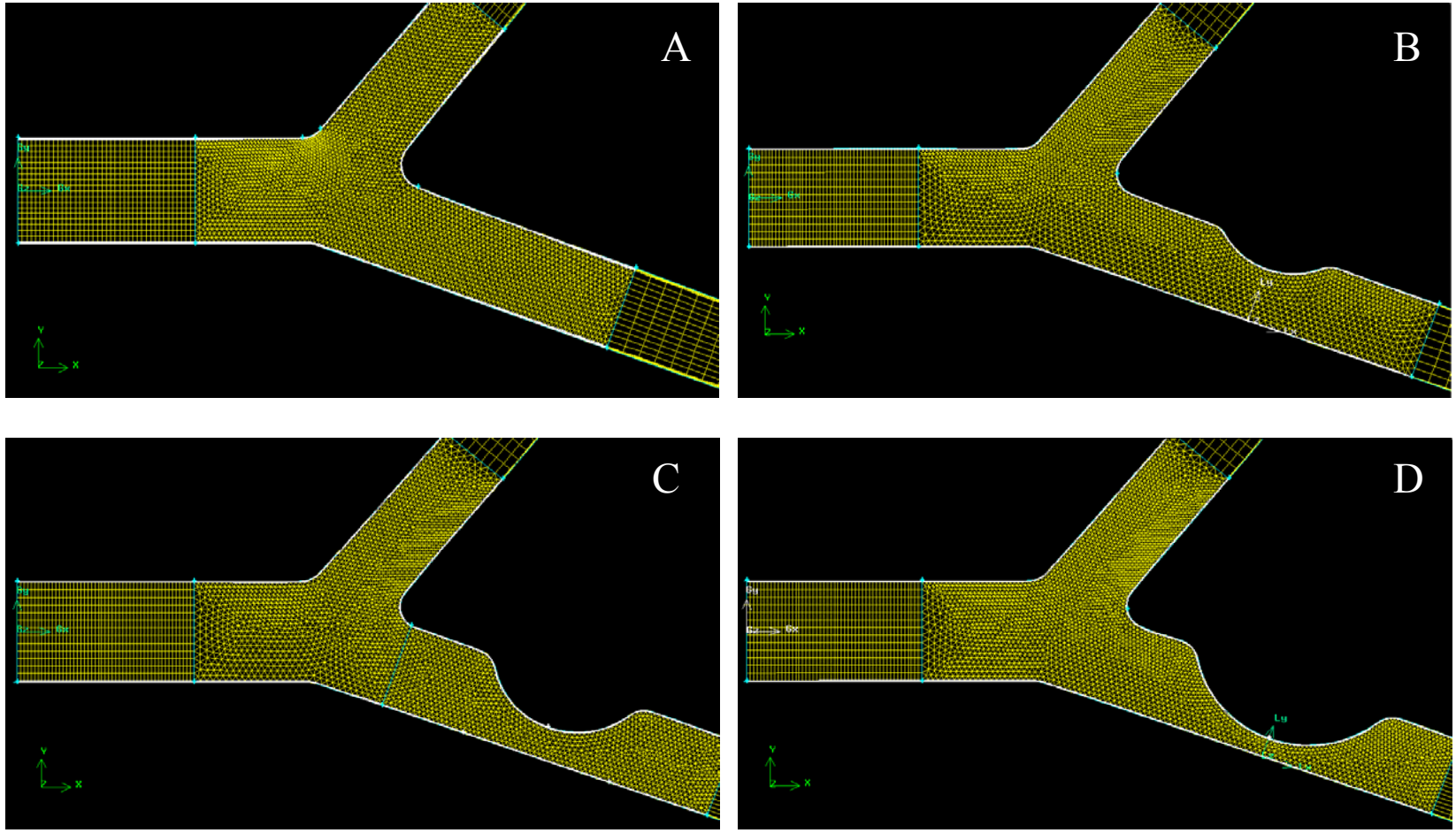

Figure 3.2 – 2D coronary artery model meshed with hybrid mesh scheme with both quadrilateral and triangular mesh elements. A – Normal condition, B – 30% stenosis condition, C – 60% stenosis condition, D – 80% stenosis condition

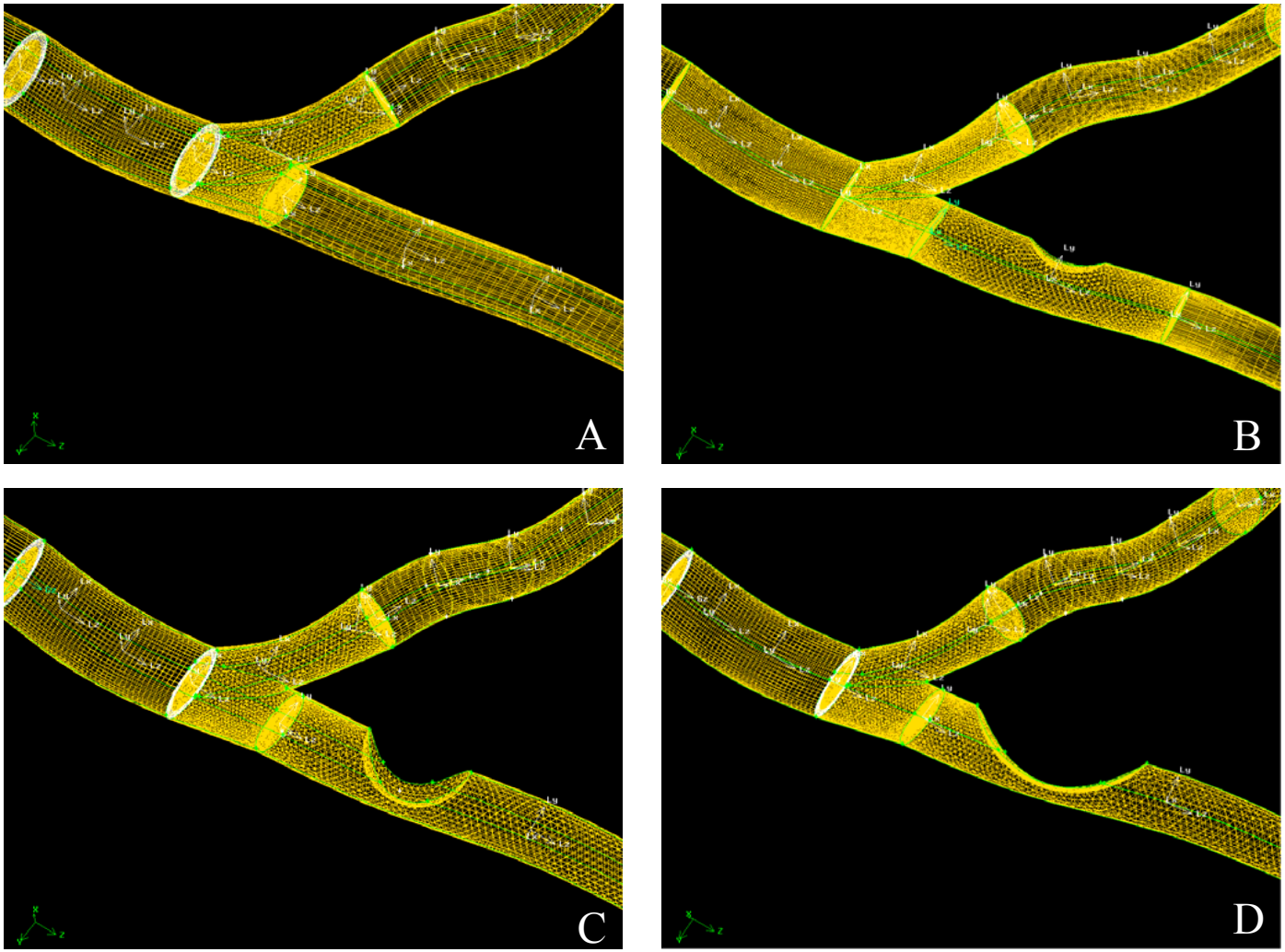

Figure 3.3 – 3D coronary artery model meshed using a hybrid scheme containing tetrahedral and hexahedral elements. A – Normal Condition, B – 30% stenosis condition, C – 60% stenosis condition, D – 80% stenosis condition

Table 3 – Total number of cells present in each model used in this study.

	2D	**3D**
Normal	14,674	412,237
30% Stenosis	25,732	694,946
60% Stenosis	30,189	331,066
80% Stenosis	30,285	353,232

3.1.3 Computational Fluid Dynamics

3.1.3.1 Basic Technique

The governing continuity and Navier-Stokes equations for incompressible Newtonian fluid were solved by the CFD solver derived from the conservation of mass and momentum equations:

$$\frac{\partial u}{\partial x}+\frac{\partial v}{\partial y}+\frac{\partial w}{\partial z}=0 \qquad (3.1)$$

$$\rho\left[\frac{\partial u}{\partial t}+u\frac{\partial u}{\partial x}+v\frac{\partial u}{\partial y}+w\frac{\partial u}{\partial z}\right]=\rho g_x-\frac{\partial p}{\partial x}+\mu\left[\frac{\partial^2 u}{\partial x^2}+\frac{\partial^2 u}{\partial y^2}+\frac{\partial^2 u}{\partial z^2}\right] \qquad (3.2a)$$

$$\rho\left[\frac{\partial v}{\partial t}+u\frac{\partial v}{\partial x}+v\frac{\partial v}{\partial y}+w\frac{\partial v}{\partial z}\right]=\rho g_y-\frac{\partial p}{\partial y}+\mu\left[\frac{\partial^2 v}{\partial x^2}+\frac{\partial^2 v}{\partial y^2}+\frac{\partial^2 v}{\partial z^2}\right] \qquad (3.2b)$$

$$\rho\left[\frac{\partial w}{\partial t}+u\frac{\partial w}{\partial x}+v\frac{\partial w}{\partial y}+w\frac{\partial w}{\partial z}\right]=\rho g_z-\frac{\partial p}{\partial z}+\mu\left[\frac{\partial^2 w}{\partial x^2}+\frac{\partial^2 w}{\partial y^2}+\frac{\partial^2 w}{\partial z^2}\right] \qquad (3.2c)$$

Where u, v and w are the three components of velocity on x, y, z directions in a Cartesian coordinate system, ρ is the density and μ is the dynamic viscosity of the fluid. P is pressure and t is time. Equations 3.1 and 3.2 (a, b, c) are for Newtonian incompressible fluids.

The basic technique involved in CFD is to subdivide the flow domain into many small regions or elements (meshing) and apply these governing equations to each of them. Solutions are obtained locally at specific locations or nodes, which are updated at subsequent time intervals over the entire domain until the required accuracy is achieved by convergence of certain variables (Chandran et al., 2007b).

3.1.3.2 Need for Turbulence solvers

A cardiac cycle (total time period of 0.9sec) generally consists of two different phases – systolic phase and diastolic phase. Figure 3.4 compares the cardiac output velocity waveform in aorta with the left coronary artery inlet velocity waveform of a

normal functioning heart with 80 beats per minute. During the systolic phase (0.3sec) the ventricular muscles contract and the blood velocity increases in arteries and during the diastolic phase (0.6sec) the muscles relax and the flow decelerates. The coronary circulation is the inverse of systemic circulation wherein maximum blood flow occurs during the diastolic phase. This is attributed to the tethering of coronary arteries to the cardiac muscles. These muscles relax during the diastolic phase thus opening up the arteries.

Winter et. al., in their study on pulsatile flow in pipes identified the conditionally turbulent flow at low critical Reynolds numbers (between 400 - 550) (Winter and Nerem, 1984). In this flow the turbulent disturbances exist during the deceleration phase but were damped by the subsequent acceleration phase. Similarly, the coronary blood flow temporarily becomes turbulent (under disease conditions) when the flow decelerates during the later part of systole (Varghese and Frankel, 2003). In a healthy artery, the effect of turbulence is usually unnoticeable. This is because the fluctuations exist for a short period of time towards the mid-to-end of systole (~ 200ms) which is followed by diastolic high velocity flow. Then the flow restabilizes and dampens the turbulence fluctuations during the succeeding systolic phase.

Apart from this, the complex flow patterns near the bifurcation region and near the stenosis region (under disease conditions) are found to create random turbulence in between cardiac cycles (Khalifa and Giddens, 1981). This underlines the need for the use of turbulent solvers to model the coronary flow.

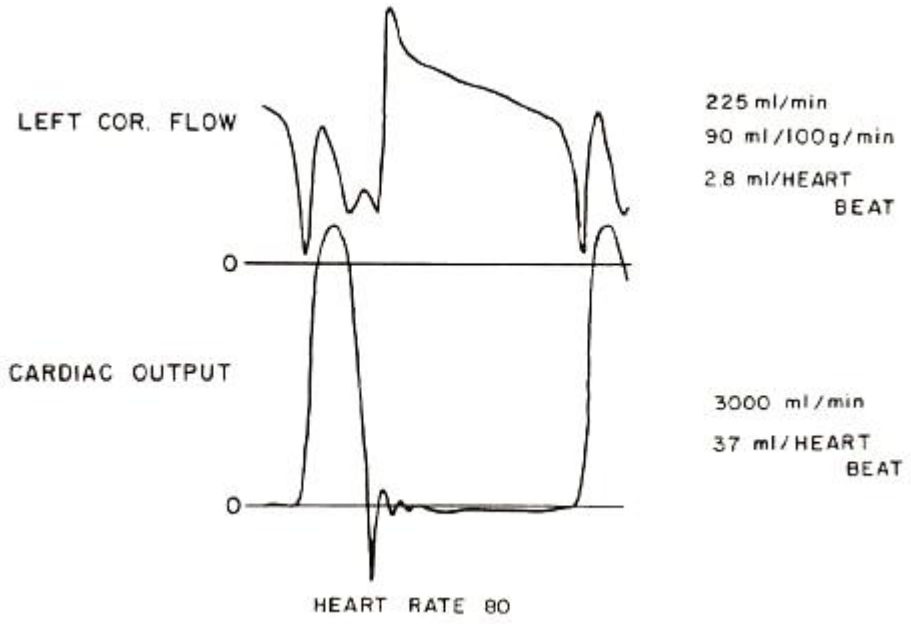

Figure 3.4 – Blood flow velocity waveform comparison between cardiac output velocity waveform in aorta (bottom curve) and in left coronary artery (upper curve). The coronary flow is the inverse of systemic flow (maximum coronary flow in diastole). (Berne et al., 1977)

3.1.3.3 Turbulent Models

The computational modeling of turbulent flow is very challenging as it exhibits unsteady and random variation. Turbulent flows are often characterized by eddies with various length and time scales. Large eddies are responsible for transport of momentum, mass, energy and other scalar quantities and they are more dependent on the geometry and the boundary conditions. Small eddies are less dependent on the geometry and are more universal.

The most popular method for analyzing turbulent flow is the Reynolds Averaged Navier Stokes (RANS) approach. The RANS equations are based on Reynolds decomposition according to which the flow variables are decomposed into mean quantity and a fluctuating quantity,

$$f(x,t) = \overline{f(x,t)} + f'(x,t) \qquad (3.3)$$

where $f(x,t)$ is the flow variable, $\overline{f(x,t)}$ is the mean component of flow variable (time-averaged) and $f'(x,t)$ is the fluctuation of flow variable from the mean value. By applying the Reynolds decomposition to ordinary Navier-Stokes equation and taking a time average results in RANS equations (Equation 3.4):

$$\frac{\partial}{\partial t}(\rho\overline{u_i}) + \frac{\partial}{\partial x_j}\left(\rho\overline{u_i}\,\overline{u_j}\right) = -\frac{\partial p}{\partial x_i} + \frac{\partial}{\partial x_j}[\mu[\frac{\partial \overline{u_i}}{\partial x_j} + \frac{\partial \overline{u_j}}{\partial x_j} - \frac{2}{3}\delta_{ij}\frac{\partial \overline{u_i}}{\partial x_i}]] + \frac{\partial}{\partial x_j}\left(-\rho\overline{u_i'u_j'}\right) \qquad (3.4)$$

In RANS approach the transport equation for the mean flow quantities are numerically solved and the scales of turbulence would be modeled. This is the major advantage of RANS approach as it reduces the computation involved in modeling complex turbulent flows. In equation 3.4 the excess term on the right hand side $\rho\overline{u_i'u_j'}$ is

called the Reynolds stress term. This is the turbulence scale term that needs to be modeled while using RANS approach. This approach is fairly efficient under transient conditions, as the fluctuations in flow variables are governed by time step (global unsteadiness) rather than by the characteristics of turbulence.

3.1.3.4 Turbulent solvers in Fluent

In Reynolds averaged approach the most commonly used model is the two-equation model. In this model the turbulent velocity and the length scales are independently calculated by solving two separate transport equations. K-ε model and K-ω model are often used to solve turbulent flow field. In these models, the first variable K (turbulent kinetic energy) determines the energy in turbulence. The second variable ε (turbulent kinetic energy dissipation) or ω (specific dissipation) determines the scale of turbulence (length/time). The standard equations for both these models were given in the following section.

The continuity equation remains the same in both the models while the momentum equation differs. Apart from this, the laminar viscosity is replaced with effective viscosity in both the models,

$$\mu_{eff} = \mu_{lam} + \mu_t$$

Where μ_{eff} is the effective viscosity, μ_{lam} is the laminar viscosity and μ_t is the turbulent viscosity. The K-ε model is not suitable for low Reynolds number turbulent flows, flows with adverse pressure gradient and flow inside the viscous sub layer (close to the wall where viscous effects are more effective than the turbulence effects). On the other hand the K-ω model is suitable for low Reynolds number turbulent flows. This model is also

efficient in solving different features of turbulence closer to the wall, in particular for flows with separation and reattachment (Wilcox, 1993).

Standard k-ε Model:

The transport equation for the K and ε derived from Navier-Stokes equations:

$$\frac{\partial}{\partial t}(\rho K) + \frac{\partial}{\partial x_i}(\rho K u_i) = \frac{\partial}{\partial x_j}\left[\left(\mu + \frac{\mu_t}{\sigma_K}\right)\right] + G_K + G_b - \rho\varepsilon - Y_M + S_K \qquad (3.5)$$

$$\frac{\partial}{\partial t}(\rho \varepsilon) + \frac{\partial}{\partial x_i}(\rho \varepsilon u_i) = \frac{\partial}{\partial x_j}\left[\left(\mu + \frac{\mu_t}{\sigma_\varepsilon}\right)\right] + C_{1\varepsilon}\frac{\varepsilon}{K}(G_K + C_{3\varepsilon}G_b) - C_{2\varepsilon}\rho\frac{\varepsilon^2}{K} + S_\varepsilon \quad (3.6)$$

Where G_k is the generation of turbulence kinetic energy due to mean velocity gradients, G_b is the generation of turbulence due buoyancy, Y_M represents the contribution of fluctuating dilatation in compressible turbulence to the overall dissipation rate, σ_K and σ_ε are turbulent prandtl numbers for K and ε, S_K and S_ε are user defined source terms.

The turbulent viscosity term (μ_t) is defined as:

$$\mu_t = \rho C_\mu \frac{K^2}{\varepsilon} \qquad (3.7)$$

The default values for the model constants are, $C_{1\varepsilon} = 1.44$, $C_{2\varepsilon} = 1.92$, $C_\mu = 0.09$, $\sigma_K = 1.0$ and $\sigma_\varepsilon = 1.3$.

Standard k-ω Model:

The transport equations for the turbulent kinetic energy and the specific dissipation rate in k-ω model derived from Navier-Stokes equations:

$$\frac{\partial}{\partial t}(\rho K) + \frac{\partial}{\partial x_i}(\rho K u_i) = \frac{\partial}{\partial x_j}\left(\Gamma_K \frac{\partial K}{\partial x_j}\right) + G_K - Y_K + S_K \qquad (3.8)$$

$$\frac{\partial}{\partial t}(\rho \omega) + \frac{\partial}{\partial x_i}(\rho \omega u_i) = \frac{\partial}{\partial x_j}\left(\Gamma_\omega \frac{\partial \omega}{\partial x_j}\right) + G_\omega - Y_\omega + S_\omega \qquad (3.9)$$

In these equations G_K and G_ω represents the Generation of turbulence kinetic energy and the generation of dissipation rate due to mean velocity gradients. Y_K and Y_ω represent the dissipation of K and ω due to turbulence. S_K and S_ω are user defined source terms. The effective diffusivity of K and ω are defined as follows:

$$\Gamma_K = \mu + \frac{\mu_t}{\sigma_K} \qquad (3.10a)$$

$$\Gamma_\omega = \mu + \frac{\mu_t}{\sigma_\omega} \qquad (3.10b)$$

The turbulent viscosity μt is defined by: $\mu_t = \alpha \frac{\rho K}{\omega}$ (3.11)

Input turbulence parameters

The input values for turbulent solvers in Fluent include the turbulent kinetic energy and the length scale. In general, turbulent length scale for a fully developed pipe flows is the hydraulic diameter at the inlet. The turbulent kinetic energy in both these models was related to turbulent intensity based on the following equation 3.12:

$$K = 1.5\, u^2 I^2 \qquad (3.12)$$

The turbulent intensity is the ratio of root mean square (RMS) turbulent fluctuations to mean velocity. The turbulent intensity is basically used as an estimate for turbulent flows based on the flow Reynolds number:

$$\mathrm{I} = 0.16(\mathrm{Re_{Dh}})^{-1/8} \qquad (3.13)$$

This equation is used to make an estimate of turbulent intensity of a fully developed core flow from which the turbulent kinetic energy can be calculated.

3.1.4 Coronary blood flow analysis

The meshed geometry of the LCA model from Gambit was imported to the CFD solver Fluent v6.3.26 (ANSYS). Every mesh was checked for presence of negative cell volumes in the grid (improper connectivity in grid) before running simulation. A segregated pressure based solver (SIMPLE algorithm) was used in all the simulations where in the continuity and momentum equations were solved simultaneously. The blood flow was solved both under steady and unsteady conditions.

Assumptions:

To solve the flow field in our models, the following assumptions were used:

- Fluid Medium: The blood was assumed to be incompressible Newtonian fluid (laminar conditions). The continuous fluid medium was modeled as blood with viscosity of 3.5cP and density 1050Kg/m^3.
- Inlet flow: The flow was modeled to be fully developed before it enters the LCA. A sufficient length of flow domain was added in front of the LCA model to ensure that the flow becomes fully developed.
- Walls: The walls of the arteries were assumed to be rigid despite the fact that the arteries are viscoelastic with the properties of flexibility, elasticity and distensibility.

The convergence criteria for all the solution variables were listed in Table 4. A minimum of 600-800 iteration was required to obtain the convergence.

Boundary Conditions:

The boundary conditions were similar for both 2D and 3D models. The boundary conditions were basically modeled in Gambit and were defined in Fluent. The boundaries were defined as follows:

- Inlet: The inlet face/edge was modeled as a velocity inlet. The velocity waveform replicating the *in vivo* cardiac pulsatile flow pattern (normal heart rate at 72bpm) as shown in Figure 3.5 was used under unsteady conditions. The unsteady velocity inlet was defined using a User Defined Function (UDF Appendix B).
- Outlet: The outlet face/edge (far downstream the flow) was modeled as pressure outlet. The flow at the outlet was set at atmospheric pressure so as to avoid any outlet effects on the results.
- Walls: The outer faces/edges were modeled as rigid non-porous walls.
- Turbulent Parameters: A uniform turbulent intensity of 3% (for fully developed internal flow) was assumed at inlet and the dissipation terms were calculated based on the length scale proportional to that of arterial diameter.
- Unsteady Condition: These simulations were run for 9 time steps with an increment of 0.1sec and the flow variables were let to converge at each time step requiring 400-600 iterations per time step.

Table 4 – Convergence criteria for solution variables used in CFD simulations.

Solution variable	**Convergence**
velocity components (x, y, z)	1.00E-06
Continuity	1.00E-06
K	1.00E-03
Omega	1.00E-03
Epsilon	1.00E-03

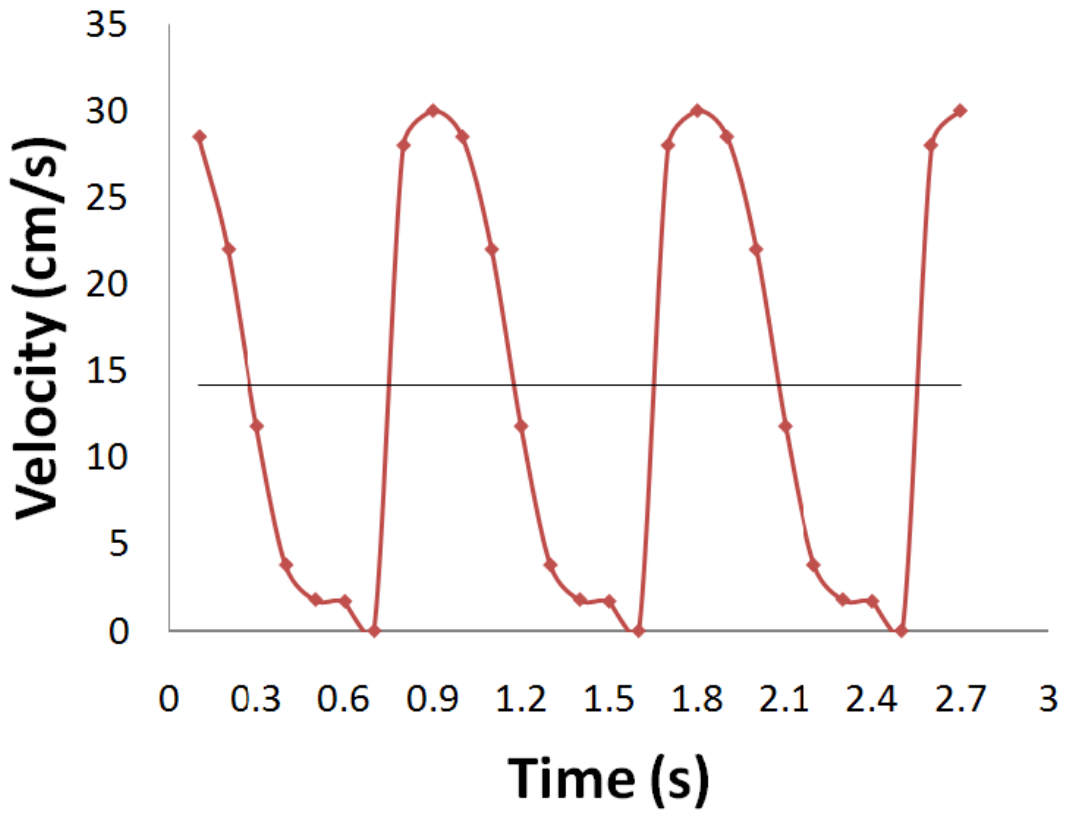

Figure 3.5 – Coronary artery inlet velocity waveform from one peak systole to other peak systole (3 cycles) of a normal human heart at 72 BPM used in CFD simulation of blood flow in coronary artery (produced based on inlet velocity waveform used in Bluestein et al. (Bluestein et al., 2002))

3.1.5 Data Analysis:

The fluent case and data files were saved after every time step once the solutions were converged. The post processing involved plotting the velocity vectors at every time step. The other major flow variables that were processed include the strain rate and effective viscosity (to calculate the shear stress). Besides, the wall shear stress (WSS) calculated by Fluent based on the velocity gradient was also processed.

These required flow variables from the converged case files were exported from Fluent in ASCII format at every time step. These ASCII files were read into Microsoft Excel to perform further analysis. For 3D iso-surface data VBA macro codes were used to convert them into matrix format. The surface plots of shear stress distribution and the wall shear stress distribution were obtained using Matlab.

3.2 *In Vitro* Studies

3.2.1 Cell Culture

Human bone marrow microvascular endothelial cells (BMEC) were obtained from Dr. Barbette Weksler (Department of Hematology and Oncology, Weill Medical College of Cornell University (New York, NY)) and were used in all *in vitro* experiments. The cells were grown on 6-well plates coated with 0.2% gelatin and used between passages 14 and 28. BMEC was cultured in Dulbecco's minimal essential media (DMEM) with 5% fetal bovine serum (FBS), 10mM HEPES, and 1:100 Penicillin/Streptomycin (10,000 unit/ml Penicillin, Final concentration is 100μg/ml and 10,000 μg/ml Streptomycin) (Invitrogen Corp.).

3.2.2 Hemodynamic Shearing Device

A hemodynamic cell shearing device based on a cone and plate viscometer was used in this study (Blackman et al., 2000). The device was custom built to use 6-well plates made of polyester and the cone was made of ultra-high molecular weight polyethylene (UHMW) material as shown in (Figure 3.6). This device is equipped with a precise microstepper motor and a motor controller system. This provides the ability to produce required shear stress uniformly to monolayers of EC grown to confluence on 6-well plates. This device was used to investigate the activation and response of EC to various shear stress conditions computed from numerical simulations.

The magnitude of shear stress generated by this device is proportional to the rotating speed of the cone. Various shear levels are obtained by adjusting the angular velocity of the cone (adjusting the microstepper motor). The cone angle used in this study is 0.5˚ and its radius is 1.733cm. The cone attached to the microstepper motor is

controlled by a BASIC computer program interfaced by a control system. The required shear stress values were first converted into angular velocity which would be programmed to the stepper motors to drive the cone. This provides the capability to create an accurate constant shear stress and a variable shear stress as regulated by the program. The entire cone and plate assembly was kept on a hot plate to maintain a temperature of 37˚ C. The microstepper motors were air cooled to avoid over heating of motors. Thus, this system provides an advantage of creating a transient shear exposure on EC similar to the shear stress history calculated from the numerical simulations.

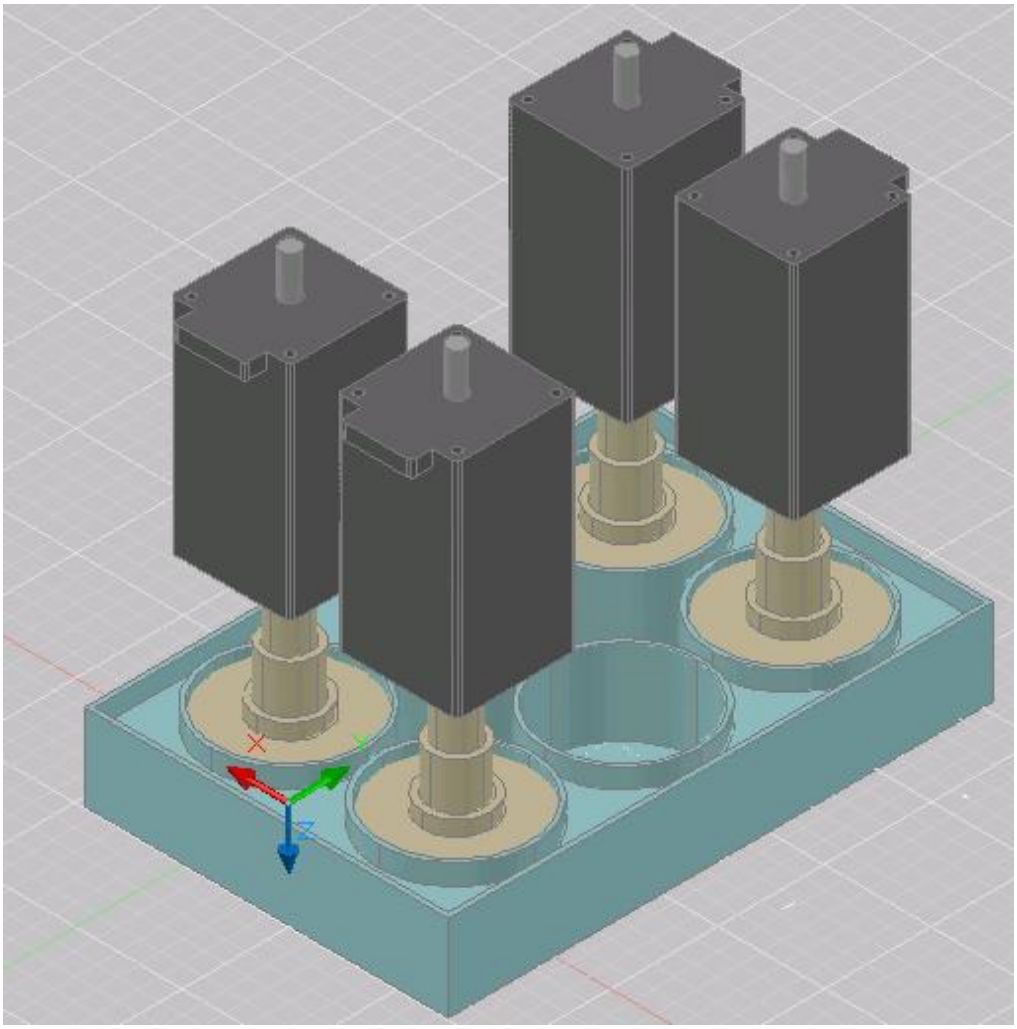

Figure 3.6 – The modified Cone and Plate hemodynamic cell shearing device showing the arrangement of cones attached to motors inside a 6-well plate used in this study.

3.2.3 Shearing Experiment

Confluent BMEC were treated overnight with normal medium containing 0.5% FBS before the shearing experiment. Constant and transient wall shear stress calculated from CFD simulation was used to stimulate BMEC. BMEC activation was measured by quantifying the amount of protein (ICAM-1 and Tissue factor) expression by cells treated at various shear levels.

3.2.3.1 Constant shear stress

A normal constant shear stress of 0.9Pa commonly found in healthy arteries (from steady CFD simulation) and a low shear stress of 0.24Pa found in recirculation zone were considered. These shear stress data from 2D stenosis condition simulation were used to activate BMEC. The two different sets of motors would apply these two different shear stress levels to the same batch of cells at the same time. A total of three sets of samples would be obtained in each experiment (four wells sheared, two as static control). One well of all three samples would be kept as control (not treated with primary antibody). The basic program used in the cone and plate controller for replicating this constant shear waveform is attached in Appendix C.

3.2.3.2 Transient shear stress

Transient wall shear stress calculated from the CFD simulations were used to activate the monolayer EC. The WSS waveforms for normal shear (healthy artery), high shear (80% stenosis throat) and low shear (recirculation zone) were programmed into the cone and plate shearing device. Similar to the constant shear experiments, three different samples including control, normal shear and high or low shear waveform were available. The waveform showed in Figure 3.7 replicates the WSS history waveform from the CFD

simulations that were programmed to the cone and plate device. These waveforms replicate the wall shear stress variation on LAD wall during normal and disease conditions assuming heart at 72 beats per minute.

The normal shear waveform varies within a shear stress range of 0.3 - 1Pa for one cardiac cycle. The low shear period within one cardiac cycle is around 0.25sec and the rest 0.65sec is the high shear period. For stenosis high shear waveform the shear range is 0.3 - 6.5Pa with the low shear period of 0.3sec and that of high shear is 0.6sec. Similarly, recirculation shear waveform has a shear range of 0.062 – 0.4Pa with the high shear period of 0.2sec and a low shear period of 0.7sec. The BASIC programs for these waveforms are attached in Appendix C.

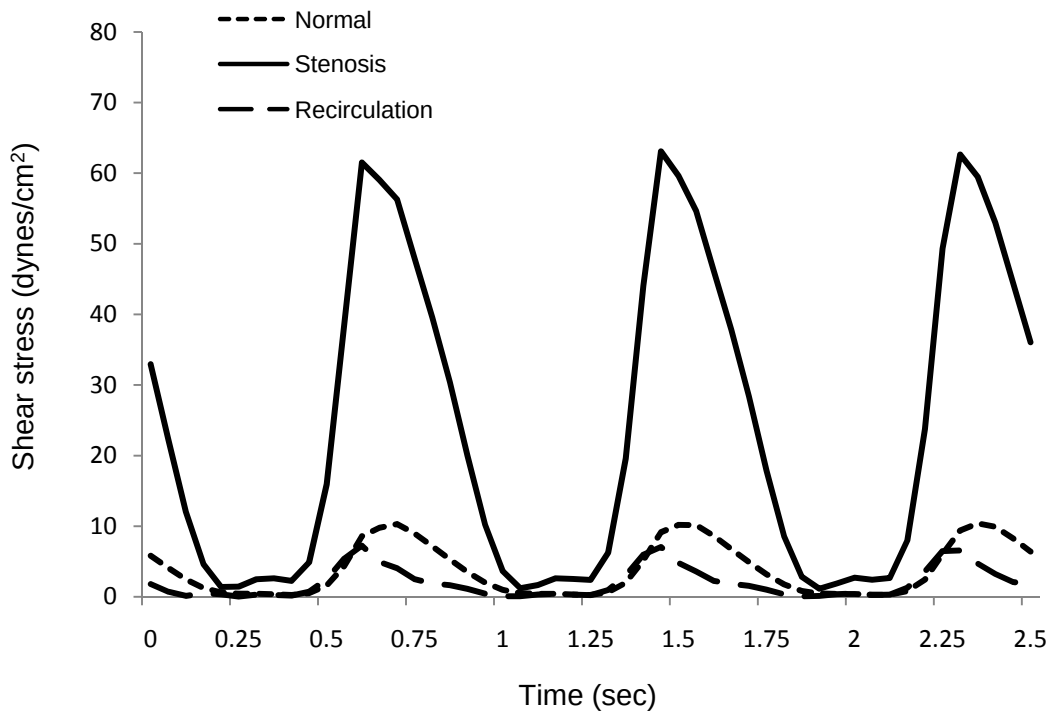

Figure 3.7 – The shear stress waveform used to replicate the real time shear stress history from CFD simulations. Normal shear was chosen from a healthy arterial location. Stenosis high shear was the WSS variation at the center point of throat. The recirculation shear was taken from a point inside the recirculation zone.

3.2.4 Protein quantification

3.2.4.1 Materials used

- 0.5% glutaraldehyde (Sigma-Aldrich)
- 100mM glycine with 0.1% BSA
- HEPES Buffered Modified Tyrode's (HBMT)

  The stock 1 contains 137mM NaCl, 2.7mM KCl, 0.36mM $NaH_2PO_4*H_2O$ and the final volume is brought to 500mLwith distilled water. The stock 2 contains 12mM $NaHCO_3$ in 500mL distilled water. The 500mL of stock 3 contains 2mM $MgCl_2*6H_2O$ and distilled water. The final HBMT solution contains 10mL stock1, 10mL stock2, 10mL stock3, 10mL of 0.2% BSA, 5.5mM of 2% dextrose and 0.01mL of HEPES Buffer (0.01M – pH 7) in 200mL of solution (pH – 7.4).
- Tris-Buffered Saline (TBS)

  TBS is made up of 19.97mM Tris and 0.15M of NaCl and in 1L of distilled water with a pH of 7.4

3.2.4.2 Sample Preparation

After shearing, the supernatant was removed and the cells were washed (2X) with TBS. EC monolayer was then fixed with 0.5% glutaraldehyde (500µl per well) for 15mins at 37˚ C. After washing (2X with TBS), cells were neutralized with 100mM glycine – 0.1% BSA (2ml per well for 30mins, 37°C). After washing (2X) with TBS, EC was then treated with the primary antibody to measure EC surface activation and inflammatory responses (37°C, 1hr). The murine monoclonal anti-human ICAM-1 antibody (1µg/ml in HBMT, Ancell Corporation, San Diego, CA) was used to measure EC activation by quantifying the amount of ICAM-1 present on the cell surface. Murine

monoclonal anti-human TF antibody (10µg/ml in HBMT, Abcam) was used to measure EC surface tissue factor expression. The primary antibody binding was detected by treating the cells with Alexa Fluor 488nm conjugated goat anti mouse secondary antibody (1:100 in HBMT) for 30min at RT.

3.2.4.3 Fluorescence Microscopy

After washing, the stained cells were examined for protein surface distribution under an optical microscope (Nikon TE 2000U). The image locations inside each well were first found using transmitted light. Then without changing the focus and stage location, the cells were imaged using fluorescent light. The images were recorded using a Coolsnap fast cooled (ES2) digital camera interfacing with NIS Elements Software under 10X magnification (Nikon, Plan Fluor DL, NA 03).

3.2.4.4 Data Analysis

The image analysis of the steady shear experiment was carried out using an image processing and analyzing software Image J (v1.4, NIH). The cell images were imported into Image J. In a particular image, three different regions of interest were selected randomly and their gray scale intensity was calculated. The intensity data was normalized by dividing the gray intensity with the area of selected region of interest and were averaged. Similar averaged data was obtained from three different locations in a particular well and were again averaged to calculate the mean normalized gray intensity. In the constant shear stress experiment, the ratio of high/low shear gray intensity to that of control (no shear) (samples from same experiment were only considered) was calculated. This was used to compare the amount of ICAM-1 and TF expressed by BMEC under different shear treatment conditions.

A Matlab (R2008a) program was used to calculate the gray scale intensity of the images from transient shear conditions. The RGB images were first converted to gray scale. Then the mean gray intensity of the entire image was calculated. The fluorescent images were then converted into black and white images based on the gray threshold intensity. The area occupied by cells in every image was calculated from this black and white image. The mean gray intensity of the image was then normalized by dividing the intensity value with the area occupied by the cells in a particular image. Similarly, data from three different locations in a particular well were averaged to obtain the normalized mean gray intensity for every shear condition. The ratio of mean gray intensity of stenosis/recirculation shear to normal shear (ratio data from same experiment) was calculated. This ratio was used to compare the amount of protein expression when BMEC were treated with shear stress levels of stenosis throat location and recirculation zone.

Similar method was used for both ICAM-1 and TF quantification. All the intensity ratio data presented in this study from both constant shear and transient shear were analyzed for statistical significance. Student's *t*-test was used and the data were considered to be significant if $P < 0.05$.

CHAPTER IV

RESULTS

4.1 Numerical Results

The computational fluid dynamic analysis was conducted on both 2D and 3D models of coronary artery under normal, 30%, 60% and 80% stenosis conditions. From this numerical simulation velocity field and the hemodynamic shear stress distribution inside the left anterior descending (LAD) branch were computed. These results were compared to analyze the hemodynamic variation between normal and disease conditions in LAD. Due to the complexity in the data set to be analyzed, iso-surfaces (diametrical cross sections perpendicular to the flow direction) were created. These surfaces were located at the regions of interest including upstream, near bifurcation and close to stenosis throat. In all the models, a steady simulation was first conducted. A maximum inlet centerline velocity of 0.3m/s was used as input condition. The results from steady simulation were analyzed to check the quality of the mesh and its spatial resolution. After checking the mesh, unsteady simulations were conducted for one cardiac cycle (duration - 0.9 sec, time step size – 0.1 sec).

The transient results revealed a huge gradient in magnitude and direction of velocity and shear stress at 800ms after systole (t=0.8 sec). This could be due to the sudden change in inlet velocity (0.01 to 0.3 cm/s). So the majority of results reported here are velocity and shear stress during 800ms after systole (8^{th} time step).

4.1.1 Velocity

The velocity vector distribution from the 2D and 3D models at t = 0.8sec are shown in Figure 4.1. The 3D vector plot is a composite picture containing vectors on all nodes inside the artery (center of picture), velocity distribution on a plane through the center of the artery (parallel to Y-axis) (bottom of the picture) and velocity profile on diametrical cross sections (perpendicular to Z axis) (top of the picture). The 2D plot contains vectors on all nodes and the velocity profile at certain cross sections (bottom of picture). The velocity profile inside the LAD (in Figure 4.1) varies significantly as disease progresses. The blood flow was fully developed (with a parabolic velocity profile - not shown) before it reached the bifurcation. This upstream parabolic flow profile (iso-surface at 5mm from inlet) was similar under both normal and stenosis conditions and also in both 2D and 3D models. The maximum centerline velocity in this cross section reached 24.5cm/sec in 3D model and 20.8cm/sec in 2D model (at t=0.8s) irrespective of normal or disease condition.

The parabolic profile became distorted as the flow approached bifurcation (iso-surface 12mm from inlet). When the flow reached the bifurcation, velocity vectors started to skew towards the inner wall with small separation zones developing near the outer walls of bifurcation (Figure 4.1). Although the velocity profile was consistently skewed towards the flow divider, the intensity and extent of skewing varied over the pulsatile

cycle. The skewed velocity profile continued into LAD for a few diameters downstream, before it became fully developed. The maximum entrance flow velocity (iso-surface 4mm from bifurcation) in LAD reached 19.65 cm/sec under normal conditions (3D model). Under stenosis conditions this value decreased as the stenosis severity increased (19.5, 18.6 and 12.6 cm/sec for 30%, 60% and 80% conditions respectively). But the entrance flow velocity in the LAD calculated from the 2D model were 14.4, 12.17, 11.51 and 11.18cm/sec under normal, 30%, 60% and 80% stenosis conditions. Despite this variation in magnitude of velocity, their distribution was similar.

To characterize the flow behavior near stenosis throat region two iso-surfaces were created. One at the center of throat (7-9mm from bifurcation) and the other within the recirculation zone (9-11mm from bifurcation). Under normal conditions with healthy artery the 2D and 3D models predicted fairly similar velocity magnitude at these locations (25.42cm/s in 2D and 24.52cm/s in 3D model). But under disease conditions these values varied significantly. The velocity vectors of all disease models revealed the flow separation near the center of throat and formation of recirculation zone just after the throat. The flow further reattached at a downstream location. However, the length and size of the recirculation zone and the point of reattachment varied based on the percentage of constriction and inlet velocity. This created a highly disturbed velocity distribution within the throat region. The flow reached a local maximum velocity at the throat and dropped to a local minimum inside the recirculation zone. The magnitude was related to the severity of stenosis throat and the time step.

In order to characterize the transient velocity variation at the throat, the time averaged flow velocity (V_{av} - average velocity over one cardiac cycle) was calculated.

The V_{av} from both the 2D and 3D models under all conditions are listed in Table 5. The 2D model predicted a 2 fold increase in velocity at the throat region (80% stenosis) while the 3D model predicted a 3 fold increase. Also the V_{av} at recirculation zone is listed in Table 5. The velocity inside the recirculation zone of 80% stenosis dropped 3 folds as that under normal conditions.

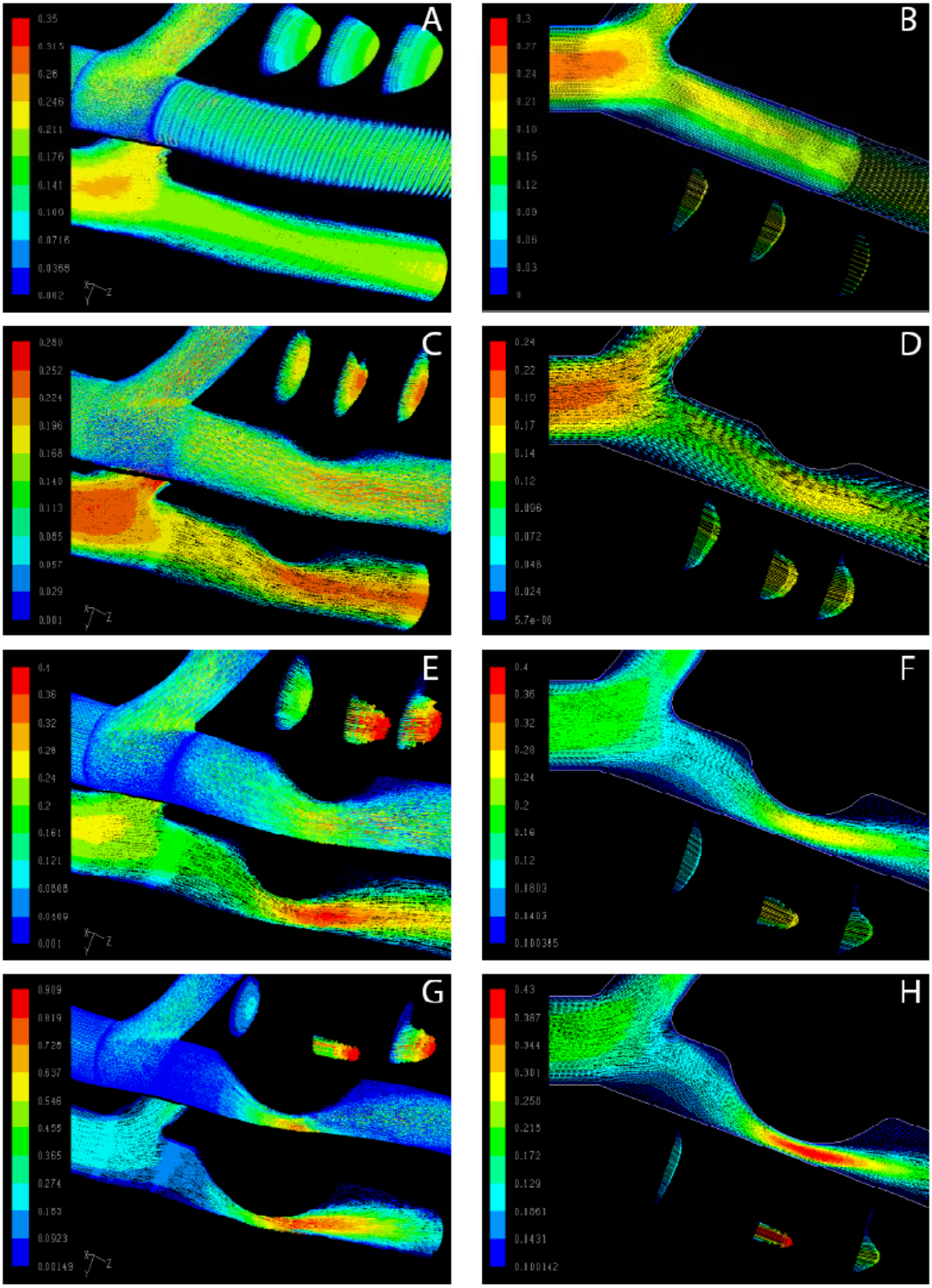

Figure 4.1 – Velocity vector distribution in LAD in 2D and 3D model during normal condition (A,B), 30% stenosis (C,D), 60% stenosis (E,F) and 80% stenosis (G,H). Vectors on all nodes (center of picture), Plane parallel to Y-axis (bottom of the picture) and velocity profile perpendicular to Z axis (top of the picture).

Table 5 – List of centerline velocity (in cm/sec) at the throat and recirculation zone during 800ms after systole (t=0.8sec). (Normal and disease conditions predicted by 2D and 3D models)

		Normal	30% Stenosis	60% Stenosis	80% Stenosis
Throat	**2D**	14.40	16.31	26.06	38.81
	3D	19.65	23.96	35.16	62.93
Recirculation	**2D**	14.25	14.67	20.97	23.51
	3D	21.94	23.71	34.39	22.62

Apart from these velocity variations, the flow was predominantly laminar under most conditions. The velocity results discussed above were estimated using both laminar and turbulent (K-Omega) solvers. The comparison of velocity magnitude estimation revealed that the laminar model was sufficient to estimate the flow field parameters in LAD under normal, 30% and 60% stenosis conditions. The maximum Reynolds number at the throat region in the above conditions was between 400 and 680. But as the stenosis severity increased (80%) the results from both the solvers significantly diverged. This could be due to the instantaneous turbulence produced near the throat at certain time step within cardiac cycle. This created a huge difference in computed velocity values, which affected other estimated parameters including wall shear stress distribution. However, the flow becomes laminar far downstream the throat region (around 15 mm from the throat center) and both the solvers computed fairly similar estimates.

4.1.2 Shear Stress

Shear stress delineates the role of hemodynamics in localization of lesions. The main objective of CFD simulation was to characterize the variation in shear stress under normal and disease conditions. The wall shear stress (WSS) on the LAD wall was calculated based on the velocity gradients in Fluent. The shear stress (SS) inside the flow field was computed based on the strain rate and local effective viscosity. Due to the huge set of data points, the iso-surfaces at specific cross sections (similar to that used in velocity estimation) were used. In transient simulations, the shear stress at different time steps was combined to illustrate the shear stress history of the flow field.

The SS distribution computed by both 2D and 3D models was fairly similar in the upstream locations. The WSS upstream the bifurcation in the LM branch remained

around 1Pa (commonly found in healthy arteries) in both the models under normal and disease conditions. Figure 4.2 is the plot of SS 10 mm before the bifurcation (at 800ms after systole) against the geometrical coordinates of diametrical cross section (Y-axis in 2D model and X-Y plane in 3D model). The SS (Figure 4.2) was symmetrically distributed with high shear on the wall gradually decreasing towards the center of lumen. The WSS on the wall at this upstream cross section varies between 0.1 and 1Pa within a cardiac cycle. As the flow reached bifurcation, the symmetrical distribution of SS was altered. The SS value calculated from 2D and 3D model started to diverge at this location (5mm before bifurcation). The time averaged SS ($\tau_{t\text{-}av}$ – average SS over one cardiac cycle in 2D; average of spatially averaged SS at a particular location over one cardiac cycle in 3D) at this location was found to be 0.32Pa from 3D model and 0.25Pa from 2D model. The shear stress pattern still remained fairly similar under normal and disease conditions. Around the bifurcation, all the outer walls experienced low WSS ($\tau_{t\text{-}av}$ between 0.1 – 0.5 Pa), while the flow divider experienced a high WSS of 3Pa (t = 0.8sec at the point of bifurcation).

The LAD wall near the bifurcation experienced a higher WSS compared to that on the other wall due to the skewed flow distribution. Figure 4.3 is the shear stress history from 2D model on the LAD wall for a length of 15mm from bifurcation. This illustrates WSS (Z axis) as a function of time (X axis) at various locations on the LAD wall (Y axis) from normal and disease condition models. Under normal condition, in both 2D and 3D models the WSS on LAD wall remained under normal levels (0.1-1Pa) downstream the bifurcation. But under disease conditions, the disturbed WSS distribution was characterized by the formation of peaks near the throat region. The stenosis throat was

modeled with its center point located approximately 8mm from the point of bifurcation. Near this location the peak WSS value (2D model) increased as the stenosis severity increased (2.4, 4.85 and 9.45Pa for 30%, 60% and 80% stenosis severity). The peak WSS value estimated by 3D model slightly varied at the throat location from the 2D model. Downstream from the throat the flow separated and a region of low WSS was formed inside the recirculation zone.

Apart from the WSS on the LAD wall near the stenosis region, the SS on the iso-surfaces (center of throat and recirculation zone) was computed. Figure 4.4 shows the SS distribution at the cross section 8mm from the LAD-LCX bifurcation (center of throat) at t=0.8sec. This figure compares the SS in both 2D and 3D models under normal and disease conditions. In general, the shear stress at the throat increased as the stenosis severity increased due to the reduction in throat diameter and increase in velocity gradient. From the 2D simulation at the throat the SS increased from 0.9Pa (normal condition) to 3.11, 6.41 and 10.5Pa under 30%, 60% and 80% stenosis respectively. The 3D model predicts similar shear distribution but the magnitude varies from 1.48Pa (normal) to 2.56, 3.23 and 14.21Pa respectively.

As we move further downstream the throat, there was a sudden change in SS distribution inside the recirculation zone. Figure 4.5 shows the SS distribution on the iso-surface located inside the recirculation zone (13mm from bifurcation) at t=0.8sec. This compares the SS distribution between 2D and 3D models. The SS on the side of recirculation zone dropped as the percentage of stenosis increased. The SS from the 2D model near the upper wall dropped from 1Pa (normal condition) to 0.1Pa (80% stenosis). The 3D model predicted a fairly similar shear levels as that of 2D model. However, the

2D model calculated a constant shear (1Pa) on the other wall while the 3D model estimated an increase as the stenosis condition increased.

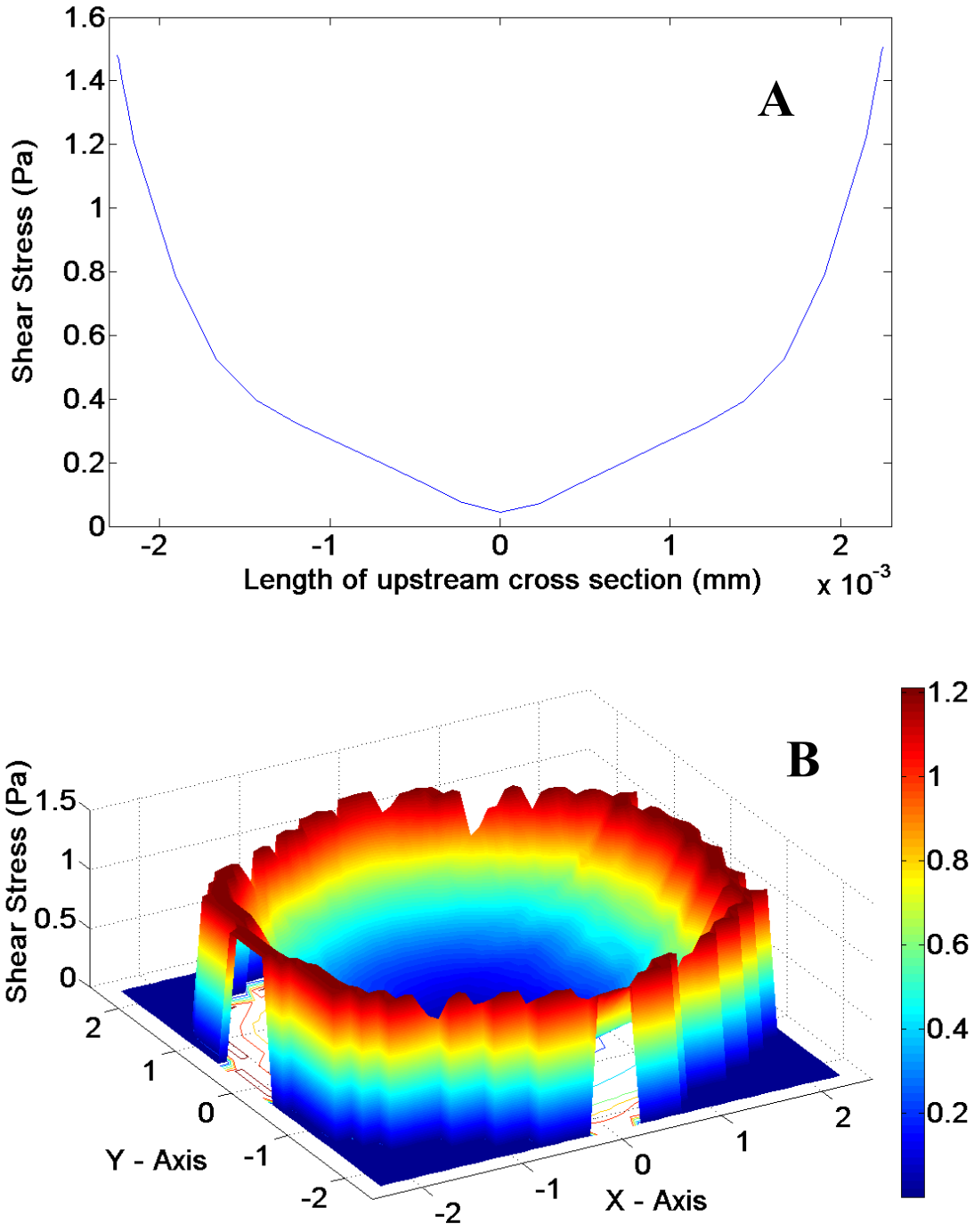

Figure 4.2 – Shear stress distribution at diametrical cross section (5mm from inlet) in the LM branch. A – Upstream cross section in 2D model; B – upstream cross section in 3D model

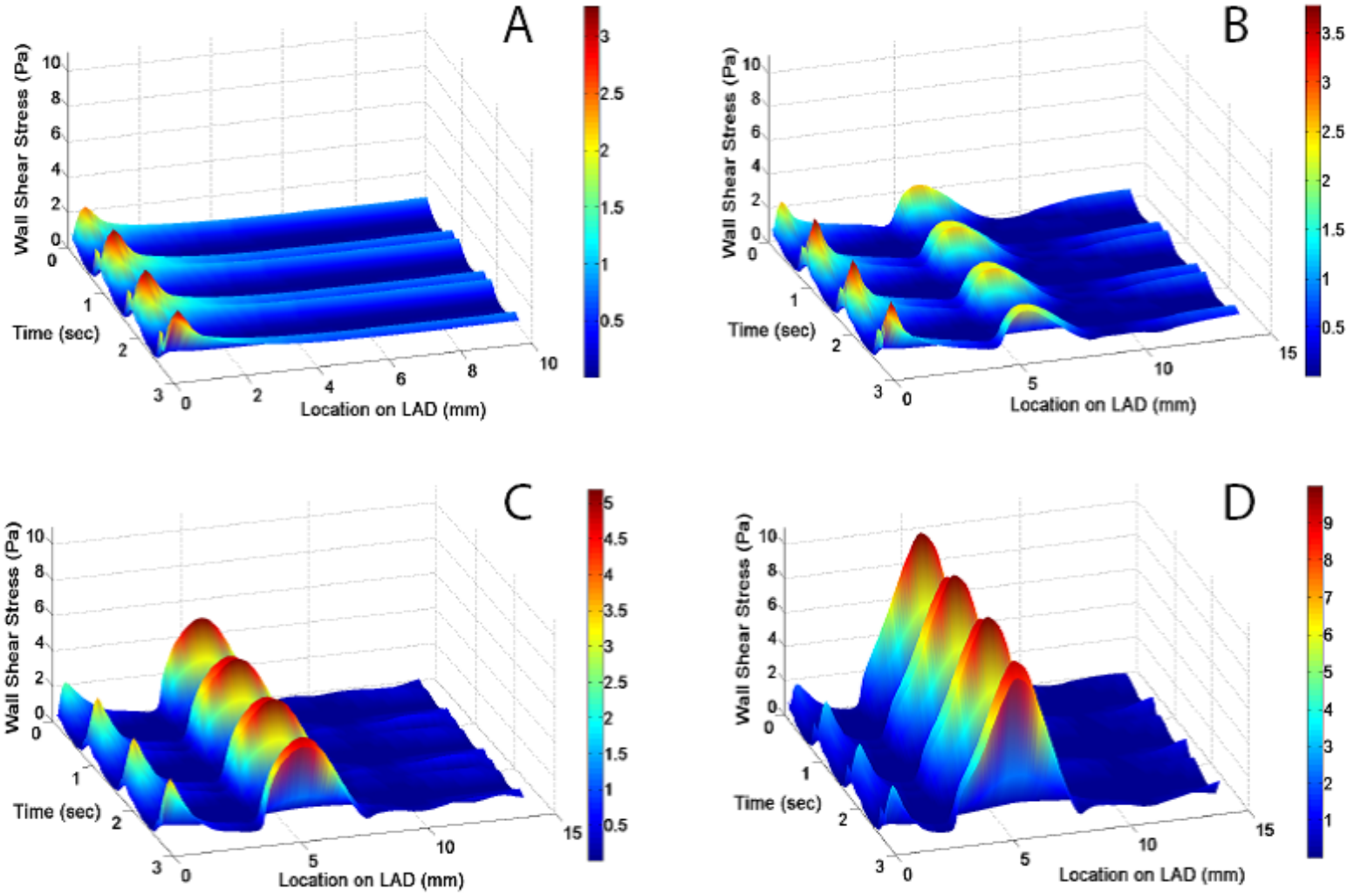

Figure 4.3 – WSS distribution on the LAD wall over three cardiac cycles. A – Normal condition; B – 30% stenosis condition; C – 60% Stenosis condition; D – 80% stenosis condition.

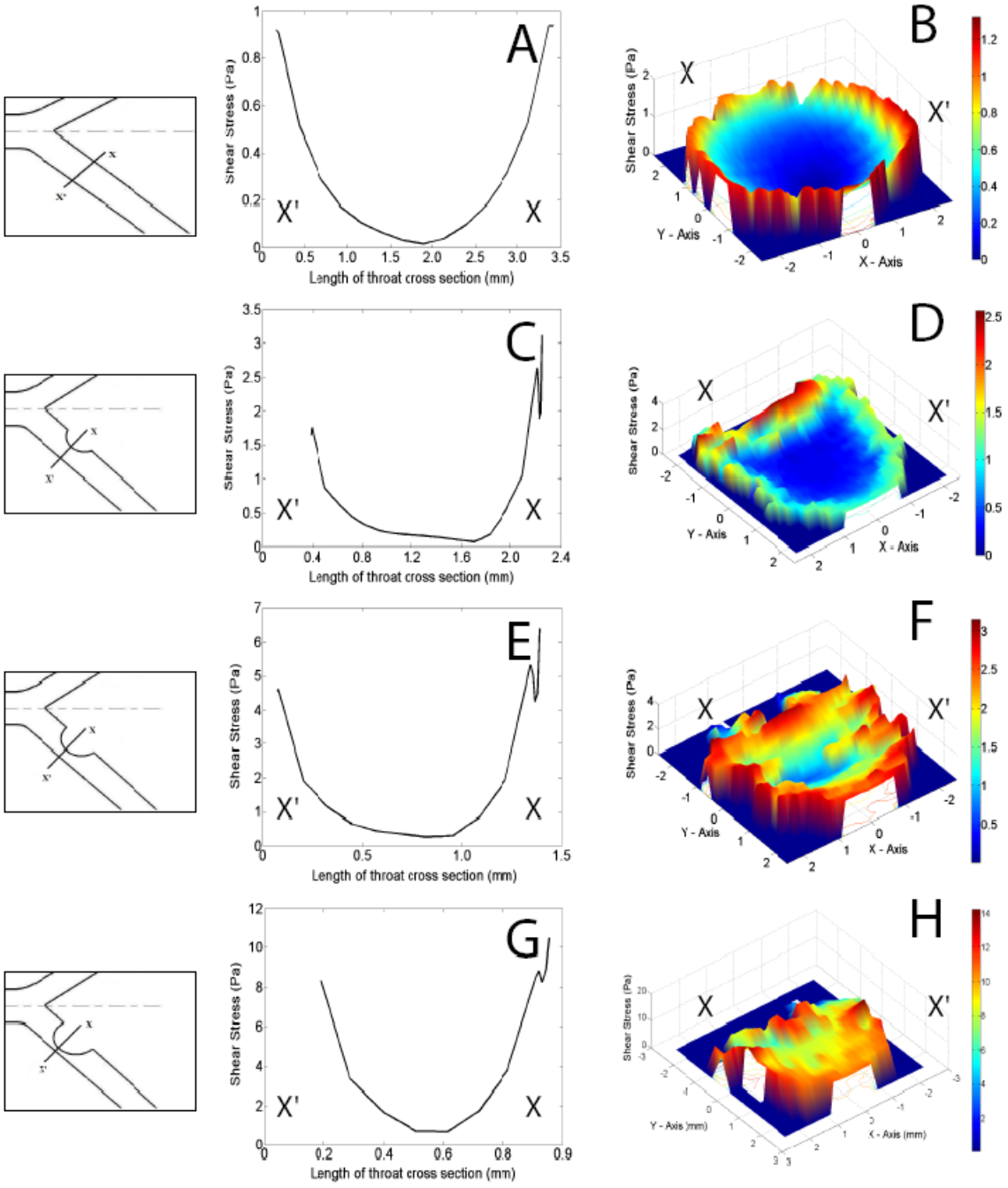

Figure 4.4 – Shear stress distribution in the throat cross section in 2D and 3D models. The upper and lower walls are marked as X and X' respectively. A, B – Normal condition; C, D – 30% Stenosis; E, F – 60% Stenosis; G, H – 80% Stenosis

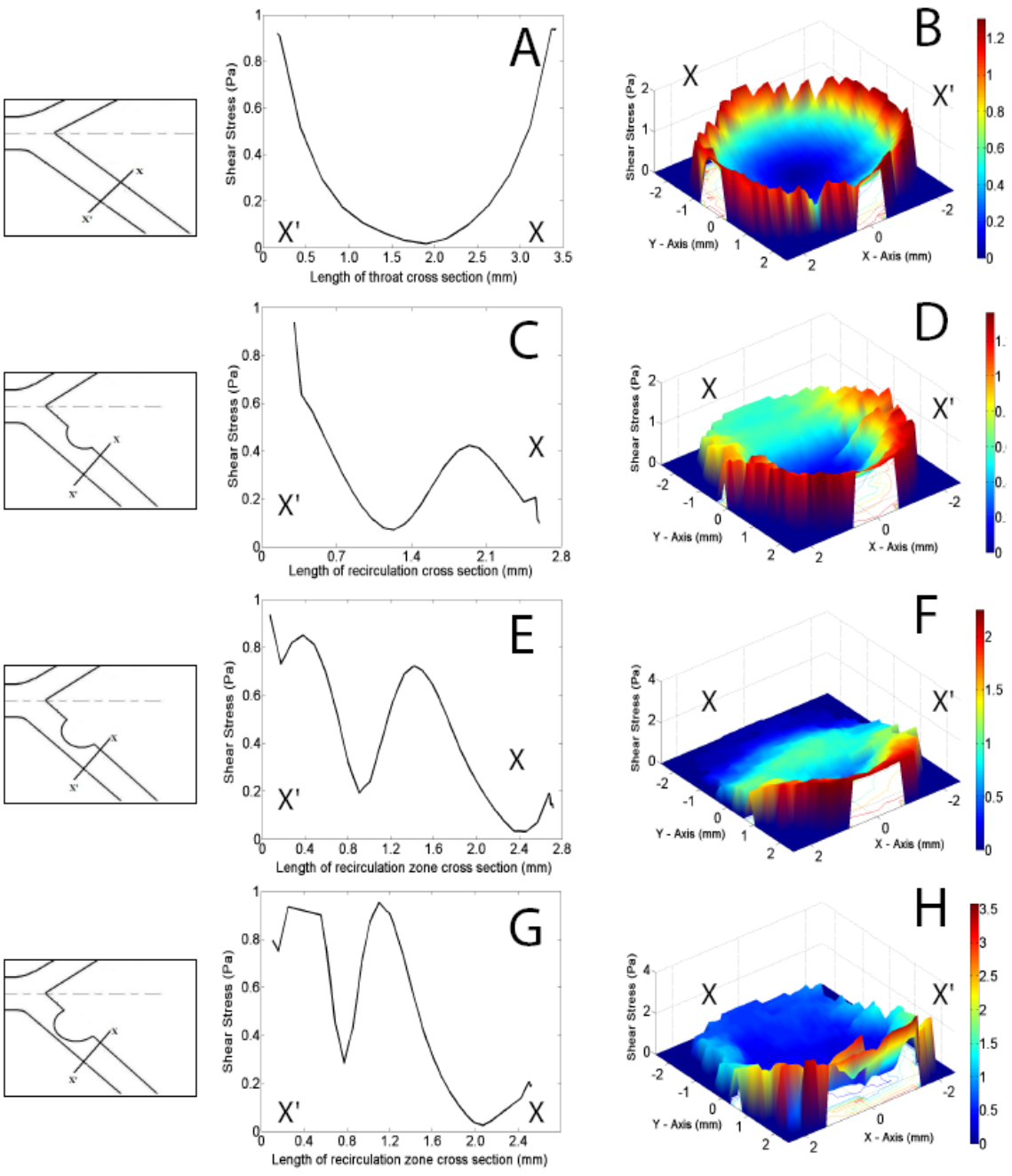

Figure 4.5 – Shear stress distribution in the recirculation cross section in 2D and 3D models. The upper and lower walls are marked as X and X' respectively. X is the location of recirculation zone. A, B – Normal condition, C, D – 30% Stenosis, E, F – 60% Stenosis, G, H – 80% Stenosis

The WSS distribution on the wall inside and outside the recirculation zone was compared. Figure 4.6 is the plot of WSS (Z axis) of various models (normal to disease conditions in Y axis) as a function of time (one cardiac cycle in X axis). This plot is based on the location maximum (τ_{max}) WSS on the recirculation wall (upper and lower) at 5mm from throat. At the location inside recirculation zone, WSS decreased from 1.1Pa under normal conditions to 0.1Pa under disease (80% stenosis) conditions. Meanwhile, the WSS on the lower wall increased from 1Pa to 3.5Pa under similar conditions. This reveals the fluctuation in shear exposure on the endothelial cells in the presence of stenosis throat.

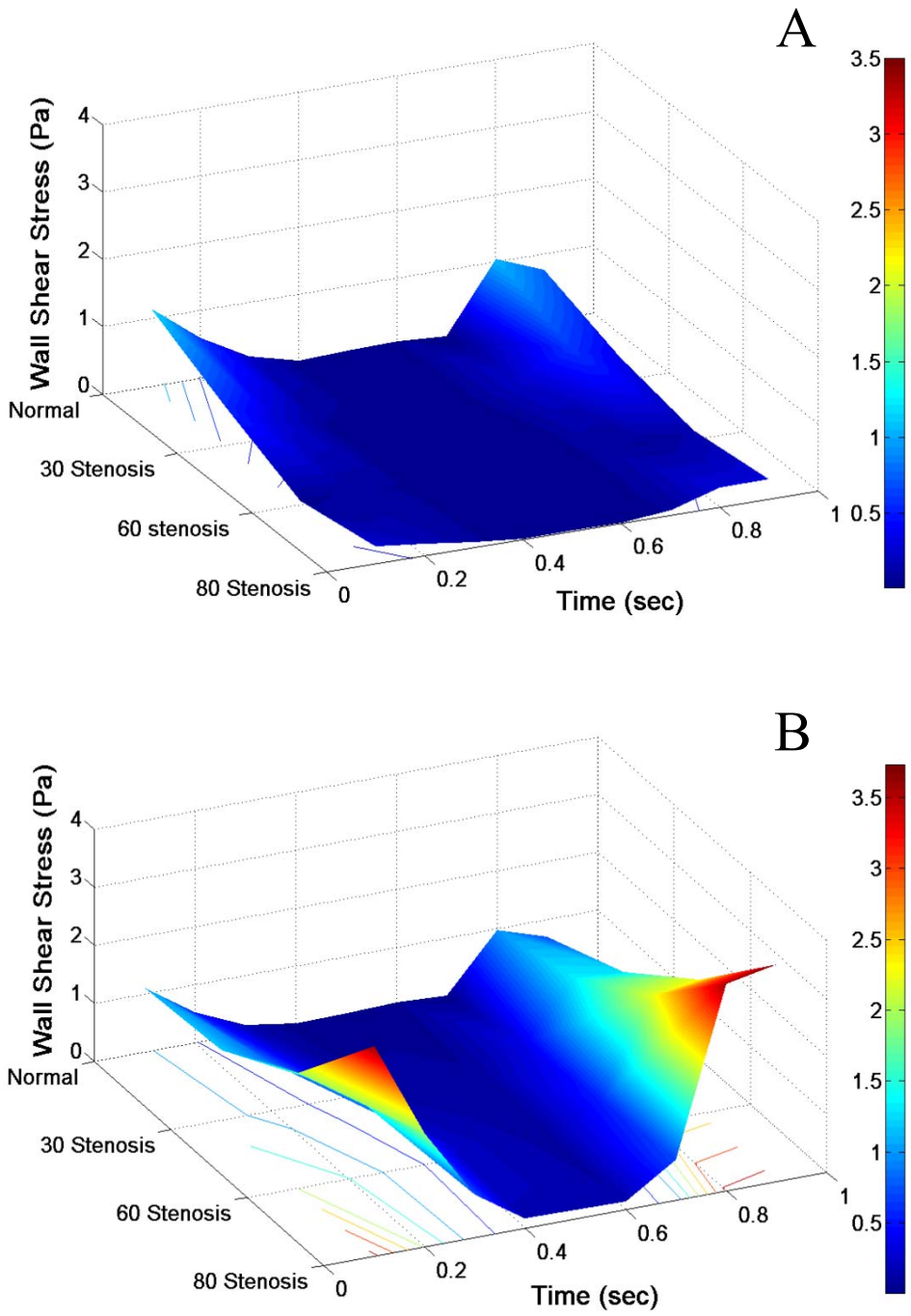

Figure 4.6 – WSS on the LAD wall at the diametrical cross section inside the recirculation zone. The plot is the variation of WSS (one cardiac waveform) at a particular location on LAD wall under normal and disease conditions. A – Upper Wall; B – Lower Wall

In order to understand the transient variation of shear exposure on the artery wall within a particular cardiac cycle, the time integral of shear stress was computed. This integral is based on the area under the shear stress – time plot. This parameter provided the estimate of shear exposure at a particular location on the LAD wall over one cardiac cycle. The shear-time integral values of all conditions are listed in Table 6.

The recirculation zone formation was characterized based on the point of flow separation and reattachment. These points varied depending on the inlet velocity and was calculated based on the change in direction of WSS distribution. Table 7 lists the length of recirculation zone in all time steps under normal and disease conditions. The length of recirculation zone reached a maximum of 1cm in 80% stenosis condition (t = 0.4 sec). At all time steps the point of flow separation remained almost the same. But the point of reattachment varied with the stenosis severity.

Also, the shear stress history (WSS waveform at a particular location) at three different locations was plotted separately (Figure 3.7). The normal arterial shear history was chosen from a normal healthy artery location. The shear variation at the center point of the throat was plotted for stenosis high shear waveform. To replicate the shear exposure to EC inside recirculation zone, the WSS variation at a particular location inside recirculation zone was plotted. These waveforms were used in the *in vitro* studies to replicate the *in vivo* shear conditions.

Table 6 – The shear stress-time integral values (Pa-s) under normal, 30%, 60% and 80% stenosis conditions in the upstream (10mm before bifurcation), before throat (4mm before throat), at throat (8mm from bifurcation) and recirculation zone (4mm from throat center).

	Normal	**30% Stenosis**	**60% Stenosis**	**80% Stenosis**
Upstream	0.495	0.4663	0.4968	0.4758
Before throat	0.4506	0.3211	0.135	0.5191
At throat	0.4321	0.8698	2.0636	4.0025
Recirculation zone	0.4147	0.1741	0.0443	0.0942

Table 7 - The length of recirculation zone (in mm) downstream the stenosis throat under 30, 60 and 80% stenosis conditions at every time step with in a cardiac cycle.

Time	30% stenosis	60% stenosis	80% stenosis
0.1	0	4	6
0.2	2	6	8
0.3	5	7	9
0.4	7	8	10
0.5	0	5	7
0.6	0	0	0
0.7	0	0	0
0.8	0	4	6
0.9	3	7	8

4.2 Experimental Results

4.2.1 Constant shear experiments

The confluent monolayers of BMEC were stimulated by a constant shear stress of 0.9Pa (normal shear stress level) and 0.24Pa (low shear stress level) for 15mins. These are most commonly found in a healthy artery and inside recirculation zones computed from CFD simulation. The sheared cells were fixed and stained against ICAM-1. Figure 4.7 shows the fluorescence microscopy images of EC activated by shear stress at 0.9Pa and 0.24Pa (10X magnification). The cells stimulated at 0.24Pa look brighter than those activated by 0.9Pa (normal shear). The morphology of cell remained elongated when exposed to low shear stress levels (0.24Pa - Figure 4.7-A). The activation of BMEC due to shear stimulation was studied based on the ICAM-1 expression on the cell surface. The surface expression of ICAM-1 distribution was quantified by estimation of the mean gray intensity of the images. The ratio of intensity of sheared to control images was used to compare the EC activation and ICAM-1 expression. The intensity ratio calculated by both the Matlab program and that of Image J are similar. Figure 4.8 shows the mean gray intensity ratio of all conditions. There was no significant increase in the amount of ICAM-1 on the cell surface when EC were sheared at 0.9Pa. Instead the cells sheared at 0.24Pa revealed a significant increase (20% increase) in ICAM-1 expression ($P < 0.05$). This reveals that the low shear stress found in recirculation zone activated the cells and increased the ICAM-1 expression compared to that of normal shear.

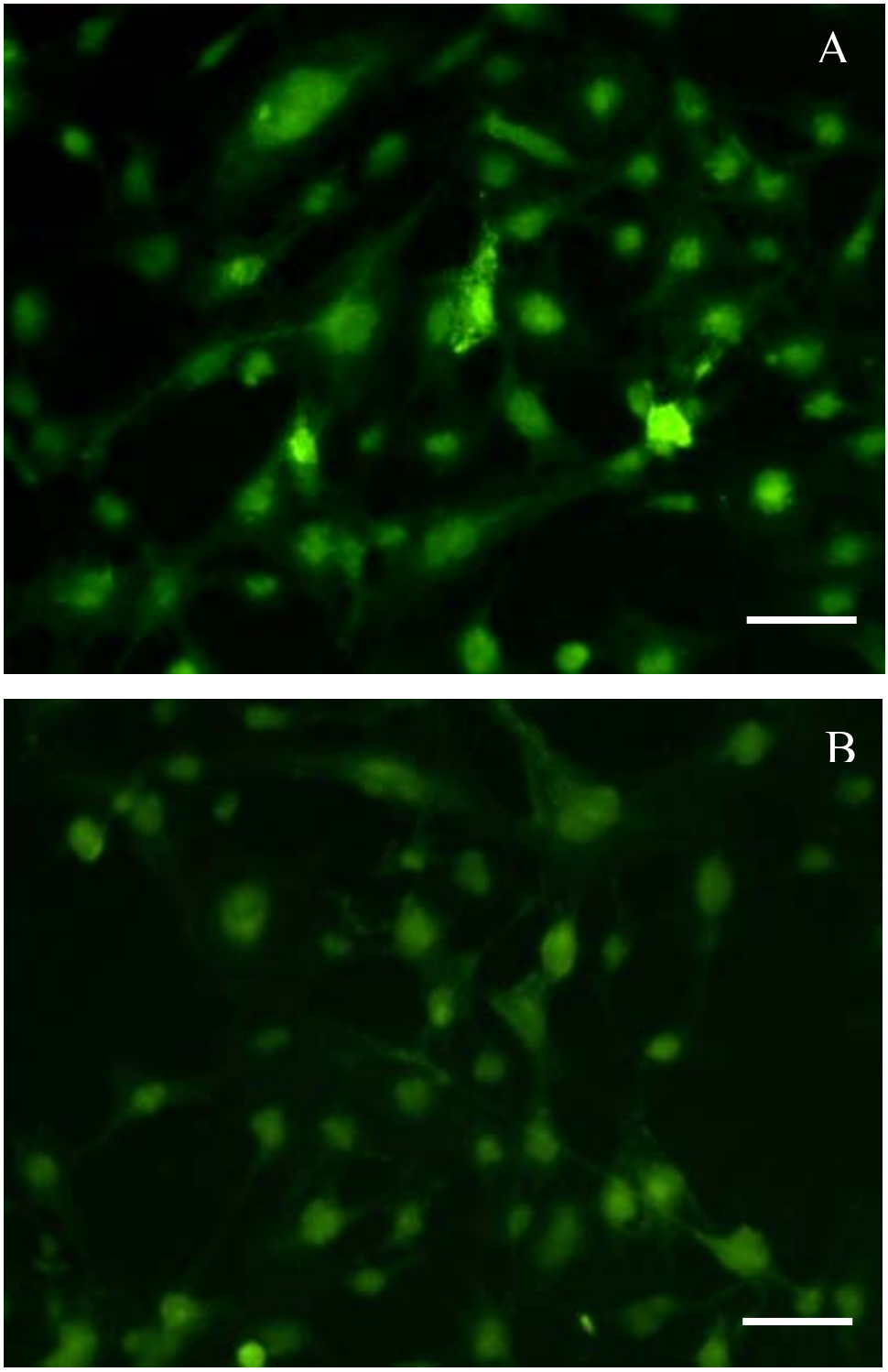

Figure 4.7 – Fluorescence microscopic image (10X magnification) of bone marrow micro-vascular endothelial cell (BMEC). A – Cells sheared at 0.24Pa; B – Cells sheared at 0.9Pa. The EC sheared at low shear levels (image A) are more activated compared those exposed to normal shear (image B). (Scale:100μm)

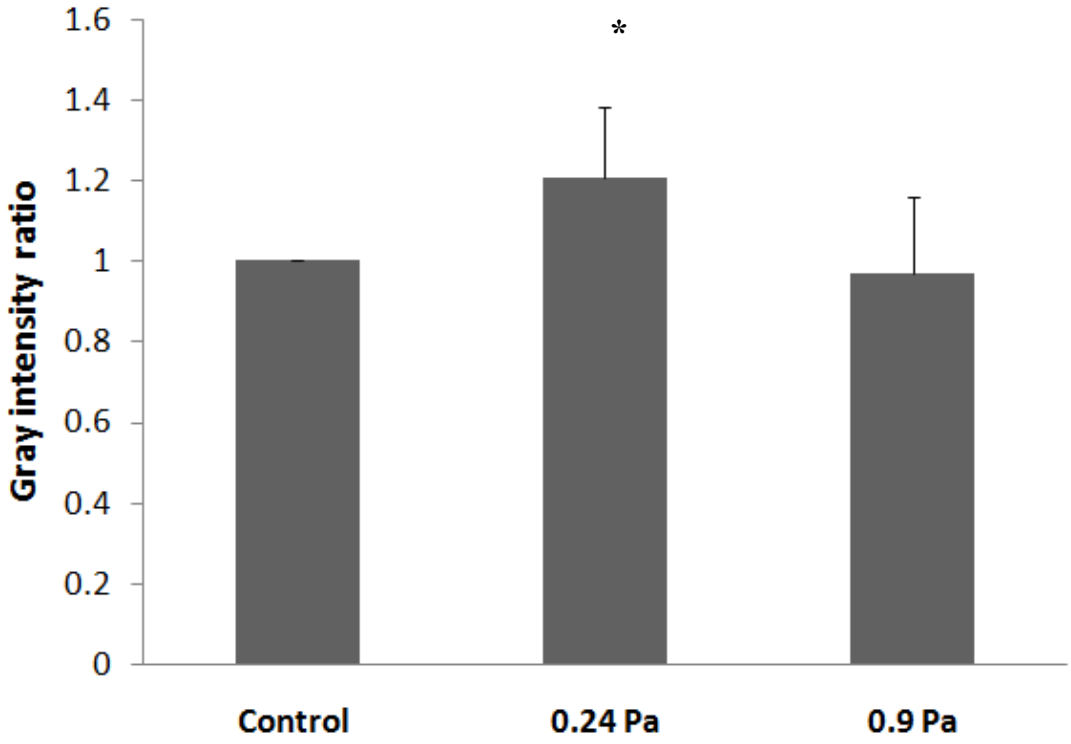

Figure 4.8 – Mean gray intensity ratio (±SEM) of control (no shear), sheared at 0.24Pa and 0.9Pa. Cells sheared at low shear stress (0.24Pa) shows significant EC activation and ICAM-1 expression compared to control and cells at normal shear stress.

* - data from 0.24Pa compared with 0.9Pa found to be significant using student *t*-test with ($P < 0.05$)

4.2.2 Transient shear experiments

The confluent monolayer of BMEC was activated by transient shear stress waveform obtained from CFD simulations (Figure in methods section). Three different WSS waveforms were used which represented the WSS distribution on LAD wall under normal shear, high shear (found in 80% stenosis throat region), low shear stress (found inside recirculation zone downstream the 80% stenosis throat). The cells were treated similar to that of the steady shear experiment and were stained for ICAM-1 and TF. Figure 4.9 shows fluorescence microscopy images of cells stained for ICAM-1 under normal shear, control (no shear), high shear and low shear (10X magnification) conditions. Cells activated by normal shear stress waveform (4.9-A) were elongated, did not align to any particular direction but made healthy connections. The cells activated by recirculation shear waveform (4.9-B) were aligned in the direction of flow along with some connections between the cells. EC exposed to high shear waveform (4.9-C) had a slightly different morphology and a preferential alignment towards the direction of flow. Similarly figure 4.10 shows images of cells stained for TF.

Based on the intensity of the ICAM-1 images (4.9), the control is (not shown) brighter than the normal shear condition. This indicates that the EC preferred normal shear and hence expressed reduced levels of ICAM-1. The stenosis high shear reduced the levels of ICAM-1 while the recirculation shear enhanced ICAM-1 expression. Based on the TF images (4.10), EC treated with stenosis high shear revealed increased TF expression compared to other images. Meanwhile, the low recirculation shear stress reduced the TF expression.

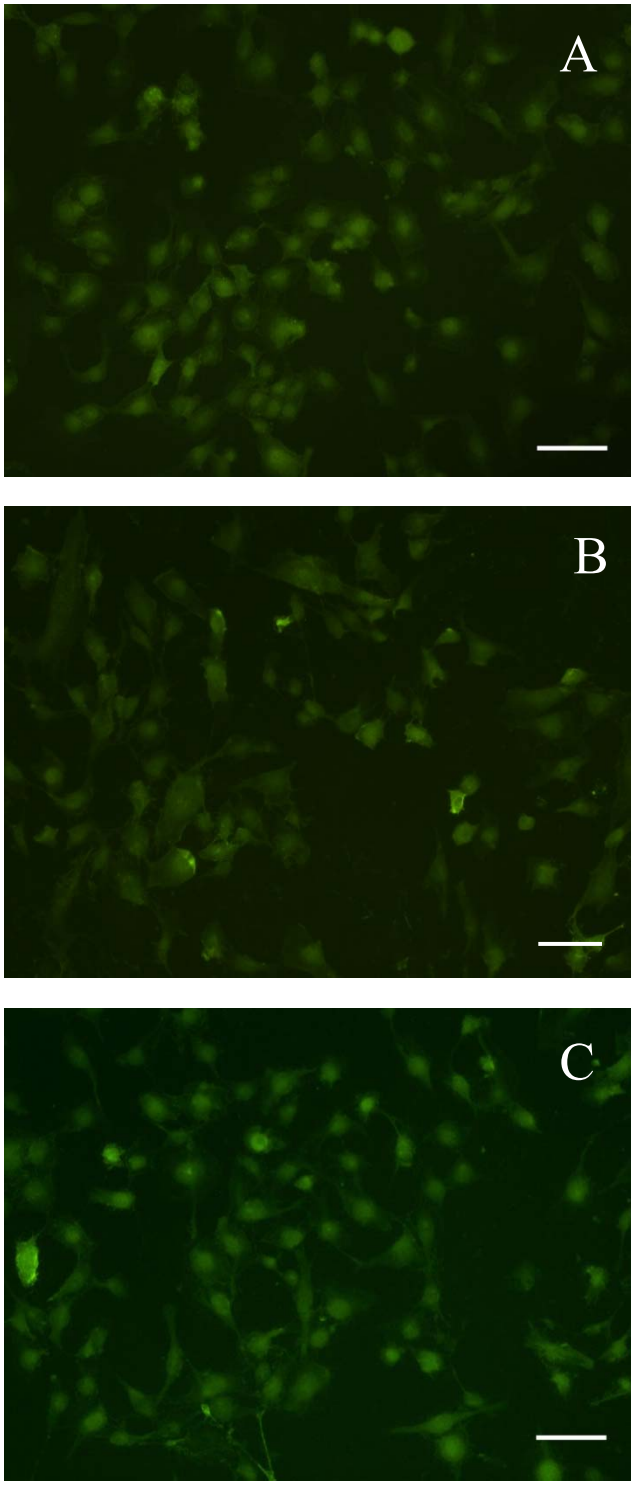

Figure 4.9 – Fluorescence microscopy images (10X magnification) of cells exposed to realistic shear stress waveform and stained for ICAM-1. A – Normal; B – stenosis throat high shear waveform and C – Recirculation zone shear waveform. The image of cells in figure C is brighter than the other images revealing that low shear enhances ICAM-1 expression. (Scale:100μm)

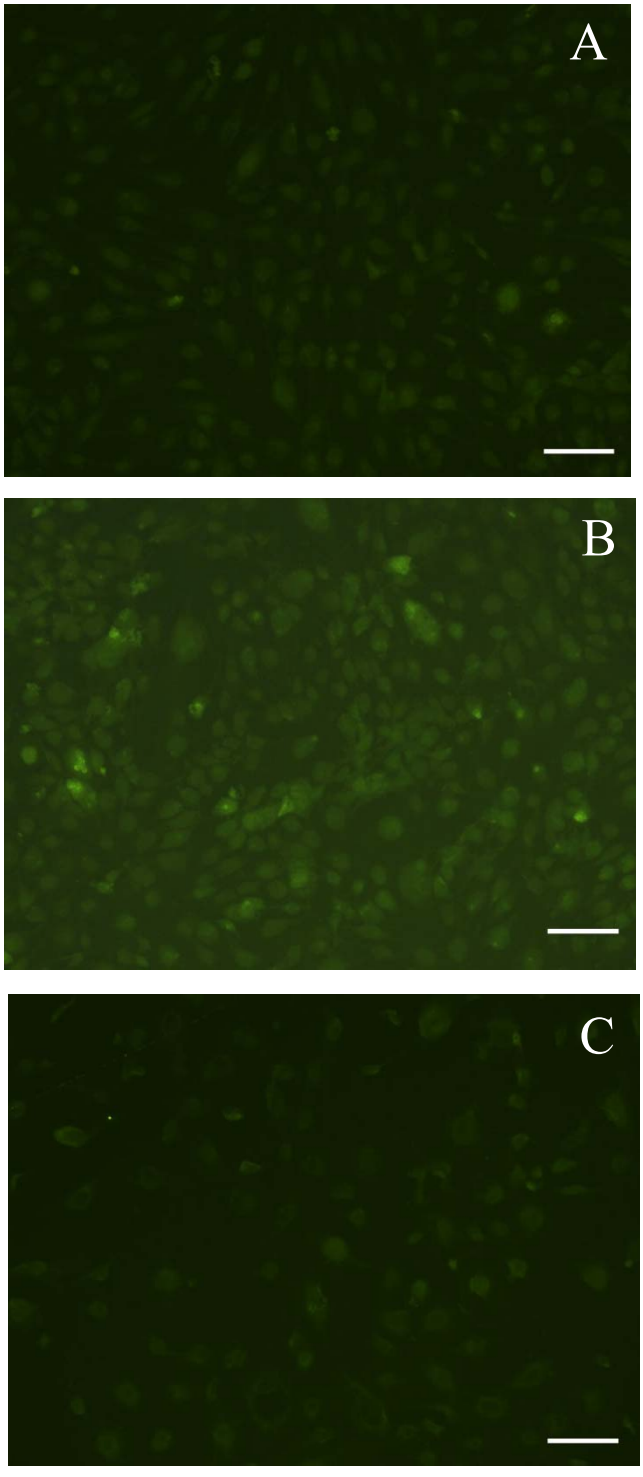

Figure 4.10 - Fluorescence microscopic images (10X magnification) of cells exposed to realistic shear stress waveform and stained for TF. A – Normal; B – stenosis throat high shear waveform and C – Recirculation zone shear waveform. B actually looks the brightest. (Scale:100µm)

The activation of EC was quantified based on immunofluorescence (for ICAM-1 and TF) similar to steady shear experiment. In this experiment, the mean gray intensity ratio was calculated based on the ratio of high shear (stenosis throat) to normal shear and low shear (recirculation zone) to normal shear. The intensity ratio calculated by both the Matlab program and that of Image J are similar. The intensity ratio of ICAM-1 in EC induced by recirculation shear stress (1.453 ± 0.322) is higher than the stenosis high shear (1.00 ± 0.123). Similarly, the intensity ratio of TF in EC induced by stenosis high shear (1.28 ± 0.317) is higher than that of recirculation low shear (1.035 ± 0.124). However, there was no statistical significance in stenosis high shear increased TF expression or recirculation low shear decreased TF expression.

CHAPTER V

DISCUSSION

Wall shear stress regulates vascular inflammatory responses and plays an important role in localization and pathogenesis of atherosclerosis. The irregular geometry of LCA creates a highly complex blood flow and the presence of stenosis intensifies the flow disturbances. The present study was intended to estimate the variation in shear stress distribution on the endothelium of a particular arterial branch (LAD) under normal and disease conditions. This study also aimed to investigate endothelial cell activation and their inflammatory responses under these shear conditions. This was achieved by a combination of numerical and experimental approaches.

5.1 Numerical Simulations

CFD is an effective tool to model arterial blood flow in complex geometries such as the left coronary artery. But the results from these numerical studies greatly depend on the geometrical and model assumptions. Ideally, a 3D model of realistic geometry discretized with a fine mesh and boundary conditions similar to that of *in vivo* will generate accurate flow field information. However, a complex computation, a highly demanding hardware and software and elongated computation time would be required.

Practically, simplified 2D models of coronary artery involving only the required geometrical features were used under many circumstances. It is challenging to determine which numerical model to use when we want to estimate the complex flow conditions in the left coronary artery, fast and accurately.

In this study a comprehensive CFD simulation of transient and turbulent blood flow inside a physiologically realistic 3D and a simple 2D LCA model was performed. The geometrical features of the 3D model were adapted from an experimental study which presented the geometrical information (averaged data) of human LCA based on arteriography (Dodge, Jr. et al., 1988b; Dodge, Jr. et al., 1992b). The 2D model was developed based on the 3D model. Both 2D and 3D models shared similar artery length (LM, LAD and LCX), bifurcation angle, diametrical taper (LAD and LCX) and similar inlet and outlet diameters. The main variation between these models was the pericardial curvature (present in multiple datum planes) which was replicated only in the 3D model.

Apart from this comparison, the blood flow in LCA was analyzed under normal and three different disease conditions (30%, 60% and 80% stenosis severity). The numerical analysis on these models provided a complete map of complex flow patterns inside the LAD and the ensuing shear stress distribution near the atheroprone sites. The flow was fully developed with a parabolic profile before bifurcation. The centerline flow velocity upstream the bifurcation was fairly similar among various conditions of 2D (20.8 cm/sec) and 3D (24.5cm/sec) models.

In the 2D model, at the bifurcation the flow skewed towards the inner divider wall. Also, in the 3D model the flow was skewed towards the outer wall of curvature. The presence of bifurcation also caused the flow in the LAD and LCX to skew towards

the inner wall (wall closer to bifurcation) for several diameters downstream the branches. This flow distribution was consistent with results from previous studies (He and Ku, 1996). The 2D and 3D models predicted slightly different LAD entrance velocity magnitude as we moved from normal to complex stenosis conditions. This could be attributed to single plane bifurcation in the 2D model compared to a multi-planar bifurcation in the 3D model. Despite this variation in magnitude the distribution was fairly similar.

Downstream the LAD, the flow velocity predicted by 2D and 3D models under normal conditions was similar. But for 30% stenosis severity, the 2D model under estimated the velocity magnitude at the throat region (time averaged - 9.2cm/sec) compared to that calculated from the 3D model (12.8cm/sec). This variation in velocity estimation enlarged as the stenosis severity increased (refer to Table 4.1). This difference may result from the pericardial curvature present in the 3D model, which changed the flow domain near the throat region. All disease condition models, predicted flow separation and formation of recirculation zone downstream the throat region. The flow velocity dropped inside the recirculation. A similar variation between the 2D and 3D model was observed in the velocity magnitude estimation inside the recirculation zone.

Apart from the variation between 2D and 3D models, the results from laminar and turbulent (low Reynolds number K-ω model) solvers were also compared. The velocity magnitude by both these solvers under unsteady flow was in resonance in most of the cases except the 80% stenosis condition. In 3D model downstream the stenosis (80%) throat, the laminar solver over estimated the maximum velocity (time averaged - 32.15cm/sec) compared to that of a turbulent solver (time averaged - 10.69cm/sec). This

may indicate the presence of instantaneous turbulence close to the wall, which was not captured by the laminar solver during transient conditions. The velocity vectors revealed the relaminarization of flow in a downstream location under all conditions.

A number of previous studies have established the immediate influence of WSS on the endothelial cell functions. In this study, both the WSS on LAD wall and the shear stress (SS) inside the flow domain was compared in all the models. The WSS in healthy arteries is generally around 1Pa. Similar to the velocity distribution, the WSS and SS in the upstream locations were fairly similar in all conditions of 2D and 3D models. The WSS on the artery wall before the bifurcation remained around 1Pa (maximum WSS under transient condition) in both models. In one cardiac cycle the WSS varied between 0.1 – 1Pa. At the bifurcation, regions of high and low shear stress were formed due to the skewness of the flow. The peak shear stress was found at the center point of bifurcation reaching as high as 3Pa. The outer walls of bifurcation received a low wall shear stress between 0.1 – 0.5Pa (in one cardiac cycle). This pattern of high and low WSS near the bifurcation was commonly found in previous studies (He and Ku, 1996; Perktold et al., 1998). The WSS values predicted by 2D and 3D models were fairly similar under all conditions.

The flow inside the LAD branch was skewed towards the upper wall due to the presence of bifurcation upstream. This created regions of disturbed WSS on the LAD wall. Also, the SS distribution was not symmetrical with formation of high shear regions towards the upper wall. Under normal conditions (both 2D and 3D models), the WSS on the upper LAD wall (wall close to bifurcation) remained under normal levels (between

0.1 – 1 Pa). The study conducted by Perktold et al., calculated a similar shear stress magnitude and distribution on the LAD wall (Perktold et al., 1998).

As the disease condition progresses on the LAD wall, regions of disturbed WSS were formed on the LAD wall. A high WSS peak was formed at the center point of the throat, immediately followed by a region of low and oscillating WSS (inside recirculation zone). The WSS increased from 1Pa during normal condition to 9.45Pa during 80% stenosis condition. This WSS data is more physiologically relevant compared to most of the previous studies on WSS distribution in LAD under disease conditions.

The results of Nosovitsky et al., using a simple 3D curved stenosis model in a phasic flow simulation, calculated a peak WSS value of about 125Pa near the throat (75% stenosis) region towards the end of systole (Nosovitsky et al., 1997b). The study conducted by M.X. Li et al used a simplified 2D geometry under different stenosis conditions. They presented a maximum WSS of 200Pa towards the end of diastole at the throat region of 70% stenosis condition (Li et al., 2007). The other study conducted by H. Yao et al., showed a peak WSS (80% stenosis and 120˚ bend) of around 900Pa near the throat on the LAD wall (Yao et al., 2000b). The major drawback of both of these studies is that they assumed LAD as a separate artery with fully developed inlet flow neglecting the effect from the presence of bifurcation upstream.

The maximum WSS estimated in our present study was 9.45Pa (2D model) and 14.21Pa (3D model) which is found on the LAD wall near the stenosis throat (80% stenosis severity). This confirms the dependence of WSS estimation on the geometry being considered, when compared to the WSS levels from the above mentioned studies.

In one of the earliest experimental work by Fry, the effect of shear stress on endothelial cells was studied (Fry, 1968). The endothelial cell layer was damaged at a shear stress level of 40Pa. In a similar study conducted by Ramstack et al., WSS levels of 100Pa would strip the endothelial cells and enhance the process of thrombogenesis (Ramstack et al., 1979). These studies reveal that the WSS levels on the LAD wall predicted by the above discussed numerical studies were physiologically irrelevant. On the other hand, these studies support the physiological relevance of estimated shear stress levels from the present study.

Apart from the variation in SS inside LAD caused by the global unsteadiness of the flow, the presence of stenosis throat further induced the disturbances. The SS at the throat region increased as the degree of stenosis increased. The location maximum (at 800ms after systole) SS increased from 1.48 during normal condition to 14.21Pa during 80% stenosis condition (3D model). Besides this variation caused by the disease condition, the SS magnitude demonstrated a variation in results computed by 2D and 3D models. The location maximum of SS at the throat region was under estimated by 2D model (10.5Pa) compared to that of the 3D model (14.21Pa).

The flow separated downstream the throat region and formed recirculation zones. This produced a low and oscillating WSS on the LAD wall. The WSS magnitude at this location was around 0.01 – 0.5Pa (within a cardiac cycle) depending on the severity of the stenosis. The recirculation zone downstream the throat further altered the SS distribution inside LAD (low SS near upper wall and high SS near the lower wall). The 2D model predicted a constant normal shear distribution near the lower wall as the stenosis severity increased. But the 3D model predicted an increase in SS with increasing

stenosis severity. This could be attributed to the secondary flow towards the lower wall due to the presence of additional curvature in the 3D model.

5.2 Experimental studies

The bone marrow microvascular endothelial cells (BMEC) were subjected to various shear stress conditions based on the numerical simulation results. In this study we used a cone and plate hemodynamic cell shearing device to activate endothelial cells. This device was very effective and suitable for replicating the required WSS waveform. The EC activation was measured based on the amount of inter cellular adhesion molecule – 1 (ICAM-1) present on the cell surface. ICAM-1 is known to play a key role in adherence of mononuclear leukocytes to EC during initial stages of atherosclerosis.

ICAM-1 expression was analyzed in many previous studies (Nagel et al., 1994; Frattini et al., 2004; Sucosky et al., 2009; Chappell et al., 1998). But there was a huge variation in their results. Frattini et.al., reported a similar ICAM-1 distribution under both laminar and turbulent condition (Frattini et al., 2004). While Nagel et.al., reported that the laminar shear stress increased surface ICAM-1 expression on force independent manner (Nagel et al., 1994). The disturbed low and oscillating shear stress was found to have increased the ICAM-1 expression (Sucosky et al., 2009; Chappell et al., 1998). However, the major drawback of these results is that the shear stress waveform was not physiologically relevant.

In this study, EC were treated with both constant and transient shear stresses. EC expressed varying amount of ICAM-1 on the cell surface when activated by different physiological shear stress (found in stenosis throat, recirculation zone, etc.). This

provides evidence for the fact that EC activation varied based on the type and magnitude of exposed SS.

BMEC expressed a significant (n= 8, $P < 0.05$) increase in ICAM-1 expression when treated with constant low shear stress (0.24Pa - normally found in recirculation zone) for 15min. The normal shear stress (0.9Pa – found in healthy arteries) did not significantly increase the ICAM-1 expression. This indicates that wall shear stress at physiological level keep vascular wall EC from getting activated. These results also indicate that atherosclerotic lesions may tend to progress towards the downstream direction which posses the recirculation zone.

Transient shear stresses on the LAD wall under normal, high shear (stenosis) and low shear (recirculation zone) conditions were used to stimulate BMEC. In this experiment, the cone and plate shearing device replicated the CFD waveforms. EC treated with stenosis high shear waveform expressed reduced levels of surface ICAM-1 compared to normal shear. But the recirculation low shear waveform increased the ICAM-1 expression. This supports the steady low shear experiment and confirms the activation of BMEC in the recirculation zone. However, with the image analysis of transient sheared EC, no statistical significance was detected.

Apart from ICAM-1, in the transient shear experiment, the surface expression of tissue factor (TF) was also measured. TF is expressed in large quantities by an injured EC as an inflammatory response. TF plays a key role in initiating the coagulation cascade during vessel injury. Previous studies have revealed a decrease in TF expression when exposed to steady low or normal shear stress (Grabowski et al., 2001; Matsumoto et al., 1998). Also, another study by Fry et al., revealed a damage to EC when exposed to high

shear stress (Fry, 1968). This reveals that an increase in TF expression by EC would mean that the EC is activated or damaged and signs of inflammatory response.

EC treated with stenosis high shear revealed an increase in TF expression compared to other samples. Meanwhile the TF expression went down when EC were treated with low recirculation shear stress. This indicates that the EC present at the throat region of the lesion exposed to high shear express increased levels of TF. However, no statistical significance was detected.

CHAPTER VI

CONCLUSION

6.1 Conclusion

A computational fluid dynamic analysis (CFD) of blood flow in human left coronary artery was conducted. A detailed map of velocity and shear stress distribution inside the left anterior descending branch was reported. The artery was studied under normal and disease conditions (three different severities – 30%, 60% and 80% stenosis). This provided a comparison of hemodynamic properties during initiation and progression and atherosclerosis in LAD. The results indicated a disturbed shear stress distribution inside LAD under disease conditions. Also, as the disease severity increased the disturbances further enhanced and created a hemodynamically active environment. Besides, the shear stress and velocity estimation was compared between 2D and 3D models. This was conducted to establish the variation in shear stress estimation arising from the geometry of LAD considered. The 2D model was sufficient to estimate a physiologically relevant shear distribution under normal conditions. But under disease conditions, the 2D models either over estimate or under estimate the flow variables (especially shear stress). This was due to the absence of pericardial curvature in the 2D model, which is normally found in coronary arteries.

A hemodynamic cone and plate cell shearing device was used to activate the bone marrow microvascular endothelial cells (BMEC) by shear stress computed from numerical simulations. These experimental results confirmed the activation of BMEC exposed to various shear levels. The cell activation was measured based on the amount of surface protein (ICAM-1, TF) expressed by EC when exposed to shear stress. In the steady shear experiments, EC exposed to low recirculation shear stress (0.24Pa) revealed a significant increase in ICAM-1 expression when compared to normal shear stress (0.9Pa). Though the transient shear supported the steady low shear EC activation results they are not statistically significant.

These results suggest that the EC present downstream the stenosis throat (inside the recirculation zone) have a higher potential to get activated. Also, increased levels of ICAM -1 would directly increase the amount of leukocyte adhesion and trans-endothelial migration. This may lead to the atherosclerotic lesion growth towards the downstream direction. Thus the combined numerical and experimental results support our hypothesis that the disturbed wall shear stress near the stenosis throat activates endothelial cells and leads to inflammatory responses.

6.2 Recommendations

Future studies will investigate the hemodynamics of blood flow in the left coronary artery (LCA) by modeling viscoelastic, porous walls and considering the wall motion due to the pericardial presence of the artery. This will be accomplished by analyzing a combination of pressure driven flow inside these arteries and the pressure gradient induced wall motion using fluid solid interaction (FSI) solvers. This will increase the physiological relevance of the results. Also, FSI would provide information

on the circumferential strain (CS) experienced by the endothelial cells (EC) due to arterial motion. This work would aim to build a complete numerical model of coronary flow which can provide an estimate of both fluid (blood) and solid (vessel wall) dynamics during the pathogenesis of coronary heart disease. The next step would investigate the behavior of EC due to the combined effect of CS and WSS.

In addition to this, particles similar to platelets will be introduced to the continuous fluid medium using discrete phase modeling. This will provide the shear exposure information on the individual platelets under disease conditions. Further, this shear stress information will be used in cone and plate shearing device to investigate the shear induced platelet activation.

REFERENCES

Ahmed, S. A., Giddens, D. P., (1984). Pulsatile poststenotic flow studies with laser Doppler anemometry. J.Biomech. 17**,** 695-705.

Asakura, T., Karino, T., (1990). Flow patterns and spatial distribution of atherosclerotic lesions in human coronary arteries. Circ.Res. 66**,** 1045-1066.

Bargeron, C. B., Deters, O. J., Mark, F. F., Friedman, M. H., (1988). Effect of flow partition on wall shear in a cast of a human coronary artery. Cardiovasc.Res. 22**,** 340-344.

Berne, R. M., Sperelakis, N., Geiger, S. R., (1977). The Cardiovascular System. American Physiological Society, Bethesda, Md.

Bevilacqua, M. P., Nelson, R. M., Mannori, G., Cecconi, O., (1994). Endothelial-leukocyte adhesion molecules in human disease. Annu.Rev.Med. 45**,** 361-378.

Blackman, B. R., Barbee, K. A., Thibault, L. E., (2000). In vitro cell shearing device to investigate the dynamic response of cells in a controlled hydrodynamic environment. Ann.Biomed.Eng 28**,** 363-372.

Bluestein, D., Li, Y. M., Krukenkamp, I. B., (2002). Free emboli formation in the wake of bi-leaflet mechanical heart valves and the effects of implantation techniques. J.Biomech. 35**,** 1533-1540.

Buschmann, M. H., Dieterich, P., Adams, N. A., Schnittler, H. J., (2005). Analysis of flow in a cone-and-plate apparatus with respect to spatial and temporal effects on endothelial cells. Biotechnol.Bioeng. 89**,** 493-502.

Bussolari, S. R., Dewey, C. F., Jr., Gimbrone, M. A., Jr., (1982). Apparatus for subjecting living cells to fluid shear stress. Rev.Sci.Instrum. 53**,** 1851-1854.

Campbell, J. J., Hedrick, J., Zlotnik, A., Siani, M. A., Thompson, D. A., Butcher, E. C., (1998). Chemokines and the arrest of lymphocytes rolling under flow conditions. Science 279**,** 381-384.

Caro, C. G., Fitz-Gerald, J. M., Schroter, R. C., (1971). Atheroma and arterial wall shear. Observation, correlation and proposal of a shear dependent mass transfer mechanism for atherogenesis. Proc.R.Soc.Lond B Biol.Sci. 177**,** 109-159.

Chandran, K. B., Yoganathan, A. P., Rittgers, S. E., (2007a). Cardiovascular Physiology. Biofluid Mechanics. CRC Press, Boca Raton, pp. 69-114.

Chandran, K. B., Yoganathan, A. P., Rittgers, S. E., (2007b). Fundamentals of Fluid Mechanics. Biofluid Mechanics. CRC Press, Boca Raton, FL, pp. 15-26.

Chappell, D. C., Varner, S. E., Nerem, R. M., Medford, R. M., Alexander, R. W., (1998). Oscillatory shear stress stimulates adhesion molecule expression in cultured human endothelium. Circ.Res. 82**,** 532-539.

Davies, M. J., Gordon, J. L., Gearing, A. J., Pigott, R., Woolf, N., Katz, D., Kyriakopoulos, A., (1993). The expression of the adhesion molecules ICAM-1, VCAM-1, PECAM, and E-selectin in human atherosclerosis. J.Pathol. 171**,** 223-229.

Davies, M. J., Woolf, N., Rowles, P. M., Pepper, J., (1988). Morphology of the endothelium over atherosclerotic plaques in human coronary arteries. Br.Heart J. 60**,** 459-464.

Dewey, C. F., Jr., Bussolari, S. R., Gimbrone, M. A., Jr., Davies, P. F., (1981). The dynamic response of vascular endothelial cells to fluid shear stress. J.Biomech.Eng 103**,** 177-185.

Dodge, J. T., Jr., Brown, B. G., Bolson, E. L., Dodge, H. T., (1988a). Intrathoracic spatial location of specified coronary segments on the normal human heart. Applications in quantitative arteriography, assessment of regional risk and contraction, and anatomic display. Circulation 78**,** 1167-1180.

Dodge, J. T., Jr., Brown, B. G., Bolson, E. L., Dodge, H. T., (1988b). Intrathoracic spatial location of specified coronary segments on the normal human heart. Applications in quantitative arteriography, assessment of regional risk and contraction, and anatomic display. Circulation 78**,** 1167-1180.

Dodge, J. T., Jr., Brown, B. G., Bolson, E. L., Dodge, H. T., (1992a). Lumen diameter of normal human coronary arteries. Influence of age, sex, anatomic variation, and left ventricular hypertrophy or dilation. Circulation 86**,** 232-246.

Dodge, J. T., Jr., Brown, B. G., Bolson, E. L., Dodge, H. T., (1992b). Lumen diameter of normal human coronary arteries. Influence of age, sex, anatomic variation, and left ventricular hypertrophy or dilation. Circulation 86**,** 232-246.

Dustin, M. L., Springer, T. A., (1988). Lymphocyte function-associated antigen-1 (LFA-1) interaction with intercellular adhesion molecule-1 (ICAM-1) is one of at least three mechanisms for lymphocyte adhesion to cultured endothelial cells. J.Cell Biol. 107**,** 321-331.

Farmakis, T. M., Soulis, J. V., Giannoglou, G. D., Zioupos, G. J., Louridas, G. E., (2004). Wall shear stress gradient topography in the normal left coronary arterial tree: possible implications for atherogenesis. Curr.Med.Res.Opin. 20**,** 587-596.

Frangos, J. A., Eskin, S. G., McIntire, L. V., Ives, C. L., (1985). Flow effects on prostacyclin production by cultured human endothelial cells. Science 227**,** 1477-1479.

Frattini, J. C., Sessa, W. E., Sumpoo, B. E., Darik, A., (2004). Endothelial expression of ICAM is stimulated by both laminar and turbulent flow. Journal of Surgical Research 121.

Fry, D. L., (1968). Acute vascular endothelial changes associated with increased blood velocity gradients. Circ.Res. 22**,** 165-197.

Fry, D. L., (1969). Certain histological and chemical responses of the vascular interface to acutely induced mechanical stress in the aorta of the dog. Circ.Res. 24**,** 93-108.

Giannoglou, G. D., Soulis, J. V., Farmakis, T. M., Giannakoulas, G. A., Parcharidis, G. E., Louridas, G. E., (2005). Wall pressure gradient in normal left coronary artery tree. Med.Eng Phys. 27**,** 455-464.

Grabowski, E. F., Reininger, A. J., Petteruti, P. G., Tsukurov, O., Orkin, R. W., (2001). Shear stress decreases endothelial cell tissue factor activity by augmenting secretion of tissue factor pathway inhibitor. Arterioscler.Thromb.Vasc.Biol. 21**,** 157-162.

Grabowski, E. F., Zuckerman, D. B., Nemerson, Y., (1993). The functional expression of tissue factor by fibroblasts and endothelial cells under flow conditions. Blood 81**,** 3265-3270.

Guretzki, H. J., Gerbitz, K. D., Olgemoller, B., Schleicher, E., (1994). Atherogenic levels of low density lipoprotein alter the permeability and composition of the endothelial barrier. Atherosclerosis 107**,** 15-24.

He, X., Ku, D. N., (1996). Pulsatile flow in the human left coronary artery bifurcation: average conditions. J.Biomech.Eng 118**,** 74-82.

Hellum, J. D., (1994). Biorheology in thrombosis research. Ann.Biomed.Eng 22**,** 445-455.

Houston, P., Dickson, M. C., Ludbrook, V., White, B., Schwachtgen, J. L., McVey, J. H., Mackman, N., Reese, J. M., Gorman, D. G., Campbell, C., Braddock, M., (1999). Fluid shear stress induction of the tissue factor promoter in vitro and in vivo is mediated by Egr-1. Arterioscler.Thromb.Vasc.Biol. 19**,** 281-289.

Huo, Y., Ley, K., (2001). Adhesion molecules and atherogenesis. Acta Physiol Scand. 173**,** 35-43.

Iwami, T., Fujii, T., Miura, T., Otani, N., Iida, H., Kawamura, A., Yoshitake, S., Kohno, M., Hisamatsu, Y., Iwamoto, H., Matsuzaki, M., (1998). Importance of left anterior descending coronary artery curvature in determining cross-sectional plaque distribution assessed by intravascular ultrasound. Am.J.Cardiol. 82**,** 381-384.

Jeremias, A., Huegel, H., Lee, D. P., Hassan, A., Wolf, A., Yeung, A. C., Yock, P. G., Fitzgerald, P. J., (2000). Spatial orientation of atherosclerotic plaque in non-branching coronary artery segments. Atherosclerosis 152**,** 209-215.

Kalbfleisch, H., Hort, W., (1977). Quantitative study on the size of coronary artery supplying areas postmortem. Am.Heart J. 94**,** 183-188.

Khalifa, A. M., Giddens, D. P., (1981). Characterization and evolution poststenotic flow disturbances. J.Biomech. 14**,** 279-296.

Li, M. X., Beech-Brandt, J. J., John, L. R., Hoskins, P. R., Easson, W. J., (2007). Numerical analysis of pulsatile blood flow and vessel wall mechanics in different degrees of stenoses. J Biomech. 40**,** 3715-3724.

Lin, M. C., Almus-Jacobs, F., Chen, H. H., Parry, G. C., Mackman, N., Shyy, J. Y., Chien, S., (1997). Shear stress induction of the tissue factor gene. J.Clin.Invest 99**,** 737-744.

Lloyd-Jones, D., Adams, R., Carnethon, M., De, S. G., Ferguson, T. B., Flegal, K., Ford, E., Furie, K., Go, A., Greenlund, K., Haase, N., Hailpern, S., Ho, M., Howard, V., Kissela, B., Kittner, S., Lackland, D., Lisabeth, L., Marelli, A., McDermott, M., Meigs, J., Mozaffarian, D., Nichol, G., O'Donnell, C., Roger, V., Rosamond, W., Sacco, R., Sorlie, P., Stafford, R., Steinberger, J., Thom, T., Wasserthiel-Smoller, S., Wong, N., Wylie-Rosett, J., Hong, Y., (2009). Heart disease and stroke statistics--2009 update: a report from the American Heart Association Statistics Committee and Stroke Statistics Subcommittee. Circulation 119**,** e21-181.

Malek, A. M., Alper, S. L., Izumo, S., (1999). Hemodynamic shear stress and its role in atherosclerosis. JAMA 282**,** 2035-2042.

Martini, F., (1992). The cardiovascular system: The Heart. In: Kendric Brake, D., schiller, D., Wechsler, D. A. (Eds.), Fundamentals of anatomy and physiology. Prentice-Hall, Inc., New Jersy, pp. 633-661.

Matsumoto, Y., Kawai, Y., Watanabe, K., Sakai, K., Murata, M., Handa, M., Nakamura, S., Ikeda, Y., (1998). Fluid shear stress attenuates tumor necrosis factor-alpha-induced tissue factor expression in cultured human endothelial cells. Blood 91**,** 4164-4172.

Matthias, E., Ulrich, L., Hartmut, M., Manfred, K., (1997). Focal Expression of Intercellular Adhesion molecule-1 in human carotid bifurcation. Stroke 28**,** 77-82.

Morigi, M., Zoja, C., Figliuzzi, M., Foppolo, M., Micheletti, G., Bontempelli, M., Saronni, M., Remuzzi, G., Remuzzi, A., (1995). Fluid shear stress modulates surface expression of adhesion molecules by endothelial cells. Blood 85**,** 1696-1703.

Motomiya, M., Karino, T., (1984). Flow patterns in the human carotid artery bifurcation.

Stroke 15**,** 50-56.

Nagel, T., Resnick, N., Atkinson, W. J., Dewey, C. F., Jr., Gimbrone, M. A., Jr., (1994). Shear stress selectively upregulates intercellular adhesion molecule-1 expression in cultured human vascular endothelial cells. J.Clin.Invest 94**,** 885-891.

Nagel, T., Resnick, N., Dewey, C. F., Jr., Gimbrone, M. A., Jr., (1999). Vascular endothelial cells respond to spatial gradients in fluid shear stress by enhanced activation of transcription factors. Arterioscler.Thromb.Vasc.Biol. 19**,** 1825-1834.

Nakashima, Y., Raines, E. W., Plump, A. S., Breslow, J. L., Ross, R., (1998). Upregulation of VCAM-1 and ICAM-1 at atherosclerosis-prone sites on the endothelium in the ApoE-deficient mouse. Arterioscler.Thromb.Vasc.Biol. 18**,** 842-851.

Nosovitsky, V. A., Ilegbusi, O. J., Jiang, J., Stone, P. H., Feldman, C. L., (1997a). Effects of curvature and stenosis-like narrowing on wall shear stress in a coronary artery model with phasic flow. Comput.Biomed.Res. 30**,** 61-82.

Nosovitsky, V. A., Ilegbusi, O. J., Jiang, J., Stone, P. H., Feldman, C. L., (1997b). Effects of curvature and stenosis-like narrowing on wall shear stress in a coronary artery model with phasic flow. Comput.Biomed Res. 30**,** 61-82.

Ohura, N., Yamamoto, K., Ichioka, S., Sokabe, T., Nakatsuka, H., Baba, A., Shibata, M., Nakatsuka, T., Harii, K., Wada, Y., Kohro, T., Kodama, T., Ando, J., (2003). Global analysis of shear stress-responsive genes in vascular endothelial cells. J.Atheroscler.Thromb. 10**,** 304-313.

Pedersen, E. M., Agerbaek, M., Kristensen, I. B., Yoganathan, A. P., (1997). Wall shear stress and early atherosclerotic lesions in the abdominal aorta in young adults. Eur.J.Vasc.Endovasc.Surg. 13**,** 443-451.

Penn, M. S., Rangaswamy, S., Saidel, G. M., Chisolm, G. M., (1997). Macromolecular transport in the arterial intima: comparison of chronic and acute injuries. Am.J.Physiol 272**,** H1560-H1570.

Perktold, K., Hofer, M., Rappitsch, G., Loew, M., Kuban, B. D., Friedman, M. H., (1998). Validated computation of physiologic flow in a realistic coronary artery branch. J.Biomech. 31**,** 217-228.

Pober, J. S., Gimbrone, M. A., Jr., Lapierre, L. A., Mendrick, D. L., Fiers, W., Rothlein, R., Springer, T. A., (1986). Overlapping patterns of activation of human endothelial cells by interleukin 1, tumor necrosis factor, and immune interferon. J.Immunol. 137**,** 1893-1896.

Ramstack, J. M., Zuckerman, L., Mockros, L. F., (1979). Shear-induced activation of platelets. J.Biomech. 12**,** 113-125.

Ridger, V., Krams, R., Carpi, A., Evans, P. C., (2008). Hemodynamic parameters

regulating vascular inflammation and atherosclerosis: a brief update. Biomed.Pharmacother. 62**,** 536-540.

Roos, E., Roossien, F. F., (1987). Involvement of leukocyte function-associated antigen-1 (LFA-1) in the invasion of hepatocyte cultures by lymphoma and T-cell hybridoma cells. J.Cell Biol. 105**,** 553-559.

Rothlein, R., Dustin, M. L., Marlin, S. D., Springer, T. A., (1986). A human intercellular adhesion molecule (ICAM-1) distinct from LFA-1. J.Immunol. 137**,** 1270-1274.

Sakamoto, N., Ohashi, T., Sato, M., (2006). Effect of fluid shear stress on migration of vascular smooth muscle cells in cocultured model. Ann.Biomed.Eng 34**,** 408-415.

Springer, T. A., (1994). Traffic signals for lymphocyte recirculation and leukocyte emigration: the multistep paradigm. Cell 76**,** 301-314.

Sucosky, P., Balachandran, K., Elhammali, A., Jo, H., Yoganathan, A. P., (2009). Altered shear stress stimulates upregulation of endothelial VCAM-1 and ICAM-1 in a BMP-4- and TGF-beta1-dependent pathway. Arterioscler.Thromb.Vasc.Biol. 29**,** 254-260.

Tentolouris, C., Tousoulis, D., Antoniades, C., Bosinakou, E., Kotsopoulou, M., Trikas, A., Toutouzas, P., Stefanadis, C., (2004). Endothelial function and proinflammatory cytokines in patients with ischemic heart disease and dilated cardiomyopathy. Int.J.Cardiol. 94**,** 301-305.

Tsuboi, H., Ando, J., Korenaga, R., Takada, Y., Kamiya, A., (1995). Flow stimulates ICAM-1 expression time and shear stress dependently in cultured human endothelial cells. Biochem.Biophys.Res.Commun. 206**,** 988-996.

Varghese, S. S., Frankel, S. H., (2003). Numerical modeling of pulsatile turbulent flow in stenotic vessels. J.Biomech.Eng 125**,** 445-460.

Wilcox, D. C., (1993). Turbulence modelling for CFD. DCW Industries, Inc., La Canada, CA.

Wilcox, J. N., Smith, K. M., Schwartz, S. M., Gordon, D., (1989). Localization of tissue factor in the normal vessel wall and in the atherosclerotic plaque. Proc.Natl.Acad.Sci.U.S.A 86**,** 2839-2843.

Willerson, J. T., (1995). Conversion from chronic to acute coronary heart disease syndromes. Role of platelets and platelet products. Tex.Heart Inst.J. 22**,** 13-19.

Winter, D. C., Nerem, R. M., (1984). Turbulence in pulsatile flows. Ann.Biomed.Eng 12**,** 357-369.

Yang, L., Froio, R. M., Sciuto, T. E., Dvorak, A. M., Alon, R., Luscinskas, F. W., (2005). ICAM-1 regulates neutrophil adhesion and transcellular migration of TNF-alpha-activated vascular endothelium under flow. Blood 106**,** 584-592.

Yao, H., Ang, K. C., Yeo, J. H., Sim, E. K., (2000a). Computational modelling of blood flow through curved stenosed arteries. J.Med.Eng Technol. 24**,** 163-168.

Yao, H., Ang, K. C., Yeo, J. H., Sim, E. K., (2000b). Computational modelling of blood flow through curved stenosed arteries. J Med Eng Technol. 24**,** 163-168.

Zarins, C. K., Giddens, D. P., Bharadvaj, B. K., Sottiurai, V. S., Mabon, R. F., Glagov, S., (1983). Carotid bifurcation atherosclerosis. Quantitative correlation of plaque localization with flow velocity profiles and wall shear stress. Circ.Res. 53**,** 502-514.

APPENDIX A

GEOMETRICAL INFORMATION OF LCA MODEL

Left main coronary artery

	Spherical Location		
Cross sectional Diameter (cm)	**r (cm)**	**theta**	**phi**
0.46	0.3	83	7
0.46	0.7	80	4
0.45	1.1	79	0

Left anterior descending artery

	Spherical Location		
Cross sectional Diameter (cm)	**r (cm)**	**theta**	**phi**
0.38	1.6	70	-3
0.37	2.3	63	-5
0.35	3	59	-8
0.31	4	51	-9
0.28	5.3	44	-12
0.26	6.5	39	-17
0.24	8	33	-23
0.2	10.1	30	-32
0.19	11.8	31	-40
0.17	12.2	32	-46
0.15	11.8	33	-49
0.11	11.4	34	-52

Left circumflex artery

	Spherical Location		
Cross sectional Diameter (cm)	**r (cm)**	**theta**	**phi**
0.43	1.4	86	-12
0.42	1.8	94	-24
0.41	2.2	102	-31
0.34	2.6	107	-33
0.34	3.1	116	-37
0.33	3.6	120	-41
0.33	4.1	126	-45
0.32	4.7	135	-51
0.29	5.4	141	-56
0.24	5.7	156	-67
0.22	5.9	166	-71
0.21	6.2	118	-73

APPENDIX B

UDF PROGRAM FOR CORONARY INLET VELOCITY

```
#include "udf.h"
#include "unsteady.h"
DEFINE_PROFILE(transient_velocity, thread, index)
{
face_t f;
real x[ND_ND];
real t = CURRENT_TIME;
real tc;
real v [100];
int N;
int j;
real y;
real i = N_TIME;
begin_f_loop(f, thread)
{
 y = i;
 N=t/0.84;
 tc=(t-0.84*N)*2.741;
 v [j] = -29.88+24.15*cos(tc)+44.1*sin(tc)+15.47*cos(2*tc)-24.42*sin(2*tc)-
10.33*cos(3*tc)-0.3837*sin(3*tc)+0.8866*cos(4*tc)+1.568*sin(4*tc);
      F_CENTROID(x,f,thread);
      y = x[1];
      F_PROFILE(f,thread,index) = v [j]/2;
 }
end_f_loop(f, thread)
}
```

Note: The velocity formula used in this UDF program is a Fourier series to represent the coronary inlet velocity waveform for one cardiac cycle

APPENDIX C

BASIC PROGRAM USED TO OPERATE CONE
AND PLATE SHEARING DEVICE

Constant shear stress experiment

Combination of high and low shear stress in each set of cone

```
rem x motors run at 2 rps and y motors run a 1 rps
rem x motor shear stress 2.4 dyn/cm and y motor 9 dyn/cm2

joff
sposx  0
sposy 0
accx 0
accy 0
A = 640
B = 2500
velx A
vely B
jogx
0
jogy
0
end
$
```

Transient shear experiment

Combination of normal and high shear stress distribution

```
joff
300
sposx  0
sposy 0
accx 0
accy 0

A = 83
B = 77
C = 90

D = 833
E = 574

velx A
jogx
vely D
jogy
wait 250

100
A = A + B
D = D + E

velx A
vely D
wait 10
if A > 2777 then goto 200
goto 100
```

```
200
A = A - C
D = D - E

velx A
vely D
wait 10
if A > 85 then goto 200

goto 300

end
$
```

Combination of normal and recirculation shear stress

```
joff
300
sposx  0
sposy 0
accx 0
accy 0

A = 83
B = 77
C = 90

velx A
jogx
vely A/4
jogy
wait 250
```

```
100
A = A + B

velx A
vely A/4
wait 10
if A > 2777 then goto 200
goto 100

200
A = A - C

velx A
vely A/4
wait 10
if A > 85 then goto 200

goto 300

end
$
```

VITA

SARAVAN KUMAR SHANMUGAVELAYUDAM

Candidate for the Degree of

Master of Science

Thesis: Numerical modeling of blood flow in human left coronary artery and *in vitro* study of endothelial cell activation by shear stress

Major Field: Mechanical Engineering (Biofluids)

Biographical:

Personal Data: Born in Erode, India, on July 31, 1986. Son of Saradha and Shanmugavelayudam

Education: Graduated from Jeppiaar Engineering College (affiliated to Anna University), Chennai, India in May 2007. Received a Bachelor of Engineering (B.E.) from Anna University, Chennai, in Mechanical Engineering. Completed the requirements for the Master of Science degree in Mechanical Engineering at Oklahoma State University, Stillwater, Oklahoma in May, 2009.

Experience: Graduate Teaching Assistant, from August 2007 to December 2007, Department of Mechanical and Aerospace Engineering, Oklahoma State University. Research Assistant, Biomedical Engineering Lab (BELOS), from January 2008 to May 2009

Professional Memberships: Student Member, Biomedical Engineering Society (BMES)

Name: Saravan Kumar Shanmugavelayudam Date of Degree: May, 2009

Institution: Oklahoma State University Location: Stillwater, Oklahoma

Title of Study: NUMERICAL MODELING OF BLOOD FLOW IN HUMAN LEFT CORONARY ARTERY AND *IN VITRO* STUDY OF ENDOTHELIAL CELL ACTIVATION BY SHEAR STRESS

Pages in Study: 106 Candidate for the Degree of Master of Science

Major Field: Mechanical and Aerospace Engineering

Scope and Method of Study: The major scope of this study was to estimate the wall shear stress (WSS) distribution inside the left anterior descending (LAD) artery under normal and disease conditions. The LAD models (2D and 3D models) were constructed based on previous studies. This assisted in predicting the deviation of WSS estimation due to the selection of LAD model. The WSS distribution was estimated by computational fluid dynamic analysis of blood flow in LAD using FLUENT. The other purpose of this study was to understand the activation response behavior of endothelial cells (EC) exposed to varying shear stress. A cone and plate hemodynamic cell shearing device was used to shear the EC, based on WSS information from numerical simulation. The EC activation was measured based on their inflammatory response i.e., the amount of surface protein (ICAM-1 and TF) expressed.

Findings and Conclusions: From the numerical studies, disturbed WSS distribution was found near the throat region. The WSS reached a peak value of around 14Pa at the center of throat in 80% stenosis condition. The recirculation zone formed downstream the throat possessed a low oscillating shear stress region. Besides, the 2D and 3D models estimated fairly similar results in the upstream location under normal and stenosis conditions but deviated near the throat region. It can be concluded that 2D model was sufficient for WSS estimation under normal conditions but not suggestible for disease conditions. The *in vitro* results revealed the EC activation and increased ICAM-1 expression when exposed to low oscillating shear stress (inside recirculation zone). Finally, the high WSS gradient in near the throat region and EC activation inside the recirculation zone may cause the lesion growth towards the downstream direction.

ADVISER'S APPROVAL: Dr. Wei Yin